NOVEL ELECTRODE MATERIALS FOR CARBON DIOXIDE AND DIOXYGEN REDUCTION

by

GHAZALEH GHADIMKHANI

Presented to the Faculty of the Graduate School of

The University of Texas at Arlington in Partial Fulfillment

of the Requirements

for the Degree of

DOCTOR OF PHILOSOPHY

THE UNIVERSITY OF TEXAS AT ARLINGTON

December 2013

Acknowledgements

I would like to express my deepest appreciation to my research advisor, Professor Krishnan Rajeshwar for his continuous guidance and encouragement throughout my research work.

I extend my sincere thanks and gratitude to my committee members, Professors Daniel W. Armstrong, Junha Jeon for their valuable guidance and advice.

My special thanks go to Professor Norma Tacconi for her immense patience with me, moral support, help, and valuable discussions throughout my research. I also thank all the past and present members of our research group for their contributions to my research. I also would like to thank Dr Frank Foss for his helpful advice in completion of the third chapter of my dissertation.

I especially thank my parents Monireh and Mehdi, my brother Mahan, for providing me their unending support and encouragement throughout my career and life. It was under their watchful eye that I gained so much drive and an ability to tackle challenges head on.

I thank the Department of Chemistry and Biochemistry at University of Texas at Arlington, for giving me an opportunity to follow my dream and for extending financial support for this dissertation study.

Finally, and most importantly, I would like to thank my husband Mahdi. His support, encouragement, quiet patience and unwavering love were undeniably the bedrock upon which the past four years of my life have been built. His tolerance of my occasional vulgar moods is a testament in itself of his unyielding devotion and love.

November 25, 2013

Abstract

Novel Electrode Materials for Carbon Dioxide

and Dioxygen Reduction

Ghazaleh Ghadimkhani, PhD

The University of Texas at Arlington, 2013

Supervising Professor: Krishnan Rajeshwar

In the first part of this study, solar photoelectrochemical reduction of carbon dioxide to methanol in aqueous media was driven on hybrid cupric/cuprous oxide (CuO/Cu_2O) semiconductor nanorod arrays for the first time. A two-step synthesis was designed and demonstrated for the preparation of these hybrid one-dimensional nanostructures of copper oxide on copper substrates. The first step was consisted of the growth of CuO nanorods by thermal oxidation of a copper foil at 400 °C. In the second step, a controlled electrodeposition of p-type Cu_2O crystallites on the CuO walls was performed. The resulting nanorod morphology with controllable wall thickness by adjusting the Cu_2O electrodeposition time as well as their surface/bulk chemical composition were probed by scanning electron microscopy, energy dispersive X-ray analysis, X-ray diffraction and Raman spectroscopy. Photoelectrosynthesis of methanol from carbon dioxide was demonstrated at -0.2 V vs. SHE under simulated solar irradiation on optimized hybrid CuO/Cu_2O nanorod arrays electrodes and without assistance of any homogeneous catalyst (such as pyridine or imidazole) in the electrolyte. Morphology and composition of the hybrid CuO/Cu_2O photoelectrodes were found to be crucial for efficient performance in methanol generation under solar illumination. Methanol formation, tracked by gas chromatography equipped with mass spectrometer, indicated Faradaic efficiencies of up to 95%.

In the second part of this research, the electrochemical properties of newly synthesized Flavin, - bis (2,2,2-trimethylammoniumethyl) - alloxazine dibromide, (thereafter denoted as Fl^{2+})

was studied on three different types of electrode materials including, glassy carbon (GC), gold (G) and copper / copper oxide (Cu/Cu_2O). Cyclic voltammetry (CV) was used to determine the interaction of Fl^{2+} with the electrodes in terms of redox potentials and reduction reaction control (surface vs. mass transport). The speciation and mechanistic details of the electroreduction and protonation of Fl^{2+} in aqueous electrolytes was studied at selected pHs in the range from 1 to 10. Spectroelectrochemistry was performed in integral and differential modes to determine the mechanistic details of this electroreduction process. The electrochemical reactions were carried out under dark and light conditions to observe whether or not light has any effect on the redox behavior of this compound. Also, the electrocatalytic performance of Fl^{2+} when the electrolyte was saturated with different gases such as, oxygen (O_2) or carbon dioxide (CO_2) was obtained and compared with blank runs under same electrolyte conditions but saturated with nitrogen (N_2).

Table of Contents

List of Illustrations

List of Tables

Chapter 1

Introduction

1-1 Electrochemistry

Electrochemistry is a branch of analytical chemistry that deals with the interconversion between the electrical and chemical energy. Its application in everyday life expands from batteries, controlling corrosion, metallurgy, electrolysis and even electrorefining processes in the manufacture of copper pipes carrying drinking water to households to technological advances like solar heating, electric cars and generally anything that involves energy storage.[1-3] Electrochemical measurements on chemical systems are carried out for various reasons including, acquisition of thermodynamic data about a reaction, generation of unstable intermediates like radicals, study of the formation or degradation rate of these species through spectroscopic properties and analysis of trace amount of metals and organic compound in different systems.[3] Oxidation and reduction reactions play an important role in all of these electrochemical processes. An oxidation reaction involves the loss of one or more electrons from chemical species while a reduction reaction is the gain of one or more electrons by chemical species. It is not possible to have one process without the other one and the combination of these two processes together is called redox reaction.[2] According to these definitions, the main principle of electrochemical processes is based on the movement of electrons in a system; electrons can flow from the oxidized species, which is also called the reducing agent or reductant, to the reduced species, which is also called the oxidizing agent or oxidant.[1]

An electrochemical cell typically consists of two electronic conductors called electrodes and two ionic conductors (for instance, cations and anions) in an electrolyte. An electrochemical reaction occurs at each electrode which is called half-cell reaction.

The sum of the reduction potential of the cathode and the oxidation potential of the anode in their half-cells is defined as cell potential.[2] There are two types of pathways related to electron flow in an electrochemical cell, galvanic and electrolytic processes.[1-3] The former one is when the electron flow is produced spontaneously by the reaction and converted into electricity, as it takes place in a galvanic cell, and the latter one is a non spontaneous reaction proceed by an outside source, as it happens in an electrolytic cell.[3]

Galvanic cell is an electrochemical cell in which chemical energy is converted into electrical energy. It has been used as batteries, pH meters, and fuel cells.[1,2] In the galvanic cell, as shown in Figure 1-1a, the oxidation and reduction half-reactions are connected by a wire and a salt bridge which is used to transfer the ions in solution to maintain charge neutrality in each half-cell.[4] Electrical current is created when the electron flows through the wire. Standard reduction potential of each half-cell determines the direction of the current in a cell. For a reaction to be spontaneous, the overall cell potential must be positive.[1,2]

A galvanic cell which has two equivalent half-cells of different concentrations is called concentration cell and the potential for this cell can be calculated using the Nernst equation. The Nernst equation is used to calculate the cell potential at any conditions and suggests the construction of concentration cells such as pH meters or other ion-selective electrodes.[3]

$$E = E^{\circ\prime} + \frac{RT}{nF}\ln\frac{C_O}{C_R} \qquad (1.1)$$

where E is the potential at any condition and $E^{0\prime}$ is the potential at standard condition (formal potential), R is the gas constant and T is the absolute temperature. CO and CR are the concentrations of oxidized and reduced species, respectively.[3]

Electrolytic cell, as illustrated in Figure 1-1b, is a cell that consumes electrical energy to drive non-spontaneous redox reactions affected by the imposition of an external potential.[4] So, an electrolytic cell is the inverse of a galvanic cell.[2,4] For example, a galvanic cell can be made from the spontaneous reaction of hydrogen and oxygen to produce water and electricity, but an electrolytic cell can combine water and electricity to produce hydrogen and oxygen in a non-spontaneous reaction. Commercial processes, which utilize electrolytic cells, include electrolytic production of chlorine and aluminum, electrorefining, and electroplating.[3]

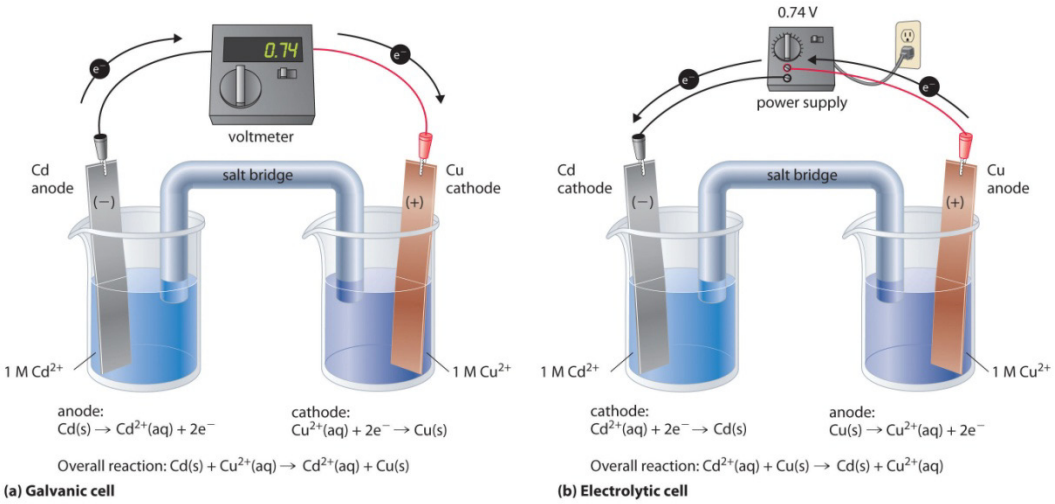

Figure1-1 Schematic diagram of galvanic and electrolytic cell (Reprinted from reference 4).

An electrochemical system consists of three different electrodes, working, counter, and reference electrode. The working electrode is the electrode in which the reaction of interest is occurring.[2,3] It is often used in conjunction with a counter electrode, and a reference electrode in a three electrode system. Depending on whether the reaction on the electrode is a reduction or an oxidation, the working electrode can be referred to as either cathodic or anodic. Gold, silver, platinum, inert carbon such as glassy carbon or pyrolytic carbon, mercury drop and film electrodes are considered as

common electrodes. For the analysis of both organic molecules and metal ions chemically modified electrodes are employed as well. The counter electrode, along with the working electrode, provides circuit over which current is either applied or measured. The potential of the counter electrode is not measured and is adjusted to balance the reaction occurring at the working electrode. This configuration allows the potential of the working electrode to be measured against a known reference electrode without compromising the stability of that reference electrode by passing current over it.[2,3] A reference electrode is an electrode which has a stable and well-known electrode potential. The high stability of the electrode potential is usually reached by employing a redox system with constant (buffered or saturated) concentrations of each participants of the redox reaction. An electrode circuit in a potentiostat is displayed in Figure 1-2.[3] This circuit functions by maintaining the potential of the working electrode at a constant level with respect to the reference electrode by adjusting the current at a counter electrode.[3,5]

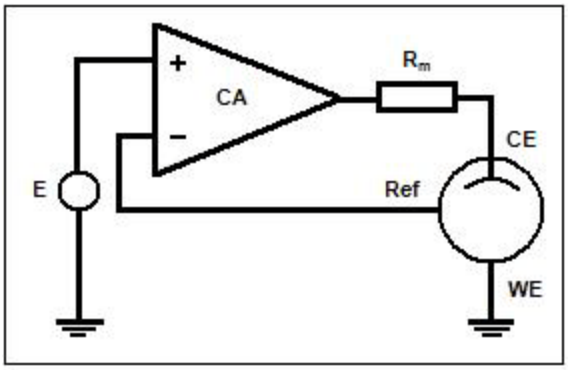

Figure 1-2 Schematic diagram of an electric circuit in a three electrode system (Reprinted from reference 3).

To understand the role of electrochemistry in different chemical reactions, variety of electrochemical methods have been developed, which can be used to study the behavior of different species in a reaction. These methods can either lead to acquisition

of quantitative information about a chemical reaction like number of electrons transferred or study the redox behavior of compounds. Electrochemical methods can be categorized in three main classes including, potentiometry, voltammetry, and coulometry.[3] Potentiometry measures the potential of a solution between two electrodes under no current flow in the system and then the measured potential is frequently used to determine the analyte quantity. Voltammetry applies a constant/varying potential at the working electrode and measures the resulting current. This method will give information about the redox potential of an analyte and its electrochemical activities. Coulometry utilizes applied current or potential to completely convert an analyte from one oxidation state to another and the total current passed is used to measure the number of electrons transferred in the system. One of the most common coulometry techniques is bulk electrolysis which will be discussed in more details.[3,5] To better understand the carbon dioxide (CO_2) reduction and mechanism and speciation of organic compounds (here flavins) some of these techniques have been discussed in more details.

Electrolysis is a common electrochemical method that can be performed under potential or current control. In controlled-potential techniques, which are the most desirable for bulk electrolysis, the potential of the working electrode is maintained constant with respect to the reference electrode. When performing a controlled-potential technique, it is better to keep the counter electrode in a separate compartment so that the reaction happening to this electrode does not interfere with the main reaction related to the working electrode surface.[3] In controlled-current techniques, the current passing through the cell is held constant. Although, these techniques frequently involve simple instrumentation than controlled-potential methods, they require either a special set of chemical conditions in the cell or specific detection methods. This method is also performed as bulk electrolysis when the electrochemical reaction is allowed to occur

completely.[3,5] In either potentiostatic coulometry or controlled current coulometry, the passage of electric current through an ionic substance incites chemical reactions at electrodes and separation of materials. Electrolysis includes chemical changes accompanying faradaic reactions, in which the amount of chemical reaction caused by the flow of current is proportional to the amount of electricity passed at electrodes in contact with electrolyte.[3] This method utilizes a large electrode area (A) to solution volume (V) ratio and generally employs a three electrode system controlled by a potentiostat as shown in Figure 1-3.[6] The working electrode is held at a constant potential and then current is monitored over time. In a process of bulk electrolysis, an analyte is converted from its original oxidation state to a new one, either reduced or oxidized depending on the applied potential.[3] As the substrate is consumed, the current decreases, approaching zero when the conversion is nearly to completion. The results of bulk electrolysis experiments are visually displayed as the total coulombs passed plotted versus time in seconds, even though the experiment measures electric current over time. This is carried out to show that the experiment approaches an expected total number of coulombs.[3] One significant use of electrolysis is the electrolysis of water which leads to production of hydrogen molecules for fuel cells and oxygen production as a fuel for space crafts and marines.[7]

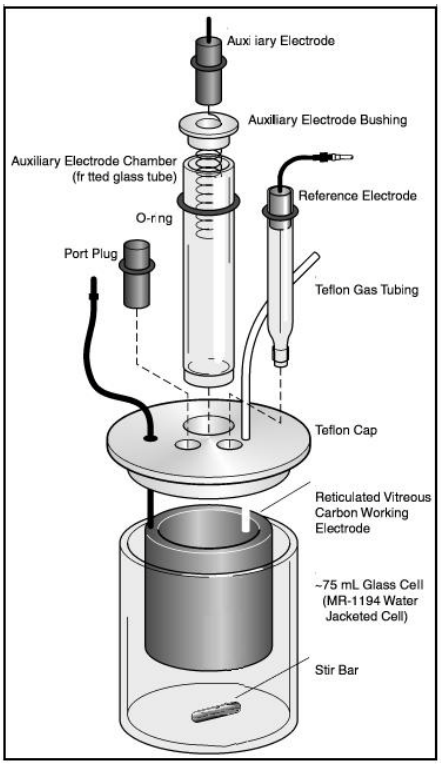

Figure 1-3 Schematic representation of a bulk electrolysis cell (Reprinted from reference 6).

Linear sweep voltammetry and cyclic voltammetry are examples of potential-sweep techniques in which the electrode potential is ramped between two potential limits at a particular scan rate while the electrode current is monitored.[3] The resulting curve is known as a voltammogram and provides information on the rate of electrochemical reactions as a function of potential. From the sweep-rate dependency of the voltammetric data, several quantitative properties of the charge-transfer reaction can be determined. Cyclic voltammetry is the most useful sweep method among other quantitative techniques for investigating electrochemical behavior of compounds.[2,3,8] It was first reported in 1938 and described theoretically by Randles.[3] In this technique, flowing current between the electrode of interest, whose potential is monitored with respect to a reference electrode, and a counter electrode is measured under the control of a

potentiostat. The voltammogram determines the potentials of different electrochemical processes occurred during chemical reactions. In a voltammetry process, the working electrode is subjected to a triangular potential sweep, whereby the potential rises from a start value, E_i, to a final value, E_f, then returns back to the start potential at a constant potential sweep rate. The applied sweep rate can vary from a few milivolts per second to a hundred volts per second. The measured current during this process is often normalized to the electrode surface area and referred to as the current density.[3,8] The current density is then plotted against the applied potential, and the result is referred to as a cyclic voltammogram. A peak in the plot of measured current versus potential shows the characteristic of any electrode reaction. The peak width and height for a particular process depends on the sweep rate, electrolyte concentration, and the electrode material. Cyclic voltammetry elucidates the kinetics of electrochemical reactions taking place at electrode surfaces.[8] Multiple peaks as well as single ones, as displayed in Figure 1-4, can be appeared in a typical voltammogram. It is possible to investigate the role of adsorption, diffusion, and coupled homogeneous chemical reaction mechanisms based on the sweep-rate dependency of the peak amplitudes, widths and potentials observed in the voltammogram.[3,8]

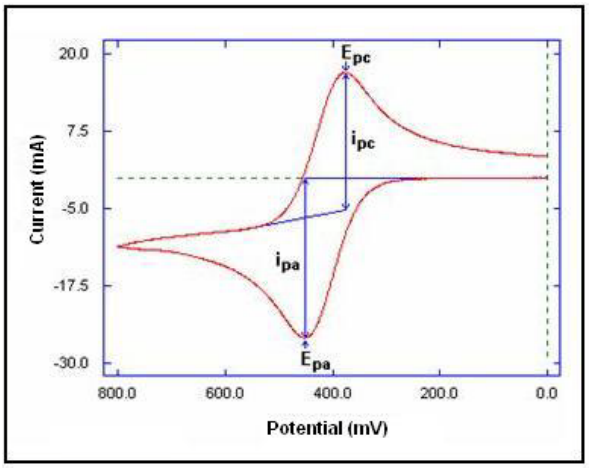

Figure 1-4 Typical cyclic voltammogram (Reprinted from reference 3).

Important parameters for a cyclic voltammogram are the peak potentials (E_p) and peak currents (i_p). If a redox system remains in equilibrium (Ox + e- ↔ Red) throughout the potential scan, it is said to be reversible. The equilibrium requires that the surface concentrations of oxidized (Ox) and reduced (Red) species are maintained at the values in agreement with the Nernst equation presented in eq. (1.1).[3]

The following parameter values are used to characterize the cyclic voltammogram of a reversible process. First, being the peak to peak potential separation *(ΔE_p)* as follows,

$$\Delta E_p = E_{pc} - E_{pa} \quad (1.2)$$

where E_{pc} and E_{pa} are cathodic and anodic peak potentials, respectively. The charge transfer will be facile, if ΔE_p equals to 58/n mV at all scan rates and 25 ^{o}C. Second, being the peak current ratio which indicates the reversibility of the redox reaction. Last, being the relationship between the peak currents and the scan rate which differentiate between a surface confined process, if the peak current is directly proportional to the scan rate, or mass transport controlled process, if the peak current is directly proportional to the square root of scan rate. For a reversible process, the peak current is given by the Randles-Sevcik equation[3] as follows,

$$i_p = 2.69\times10^5\times n^{3/2}\times A\times C\times D^{1/2}\times v^{1/2} \quad (1.3)$$

where i_p is the peak current in amperes (A), n is the number of transferred electrons, A is the electrode surface area in cm^2, C is the concentration of the analyte in the sample in molarity, D is the diffusion coefficient in cm^2/s and v is the kinematic velocity in cm/s. Formal potential, $E^{o\prime}$, is given by the mean of the peak potentials.[3,5]

In order to study the mechanism of different types of compounds in more detailed manner, spectral techniques can be coupled with electrochemical methods to give better understanding of the redox reactions. Spectroelectrochemistry is a powerful method to continuously analyze variety of compounds and study the behavior of different species through the passage of light and electricity. It is a combination of electrochemistry and spectroscopy to study the redox chemistry of organic and inorganic compounds. In other word, the oxidation states of the compounds are changed electrochemically by addition or removal of electrons at the electrode surface while spectral measurements in the solution corresponds to the species which are simultaneously formed. Such techniques are convenient means for obtaining spectra and redox properties of different groups of complexes.[3]

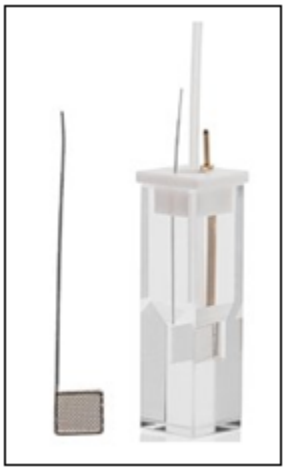

Figure 1-5 Schematic illustrations of the spectroelectrochemical cell and the platinum minigrid working electrode (Reprinted from reference 9).

One of the simplest spectroelectrochemical experiments is to use a light beam in the UV-Visible range where the beam directly goes through the electrode surface and the changes in the absorbance due to the formation or disappearance of different

compounds is measured simultaneously. One of the main requirements for these experiments is an optically transparent electrode (OTE). There are several types of OTEs including, thin films of semiconductors, metal deposited on glass, quartz or plastic substrate, and fine wire mesh, *minigrids*, with several hundred wires per centimeter.[3] Figure 1-5 is a display of the electrochemical cell with a platinum minigrid as working electrode.[9]

In conclusion, spectroelectrochemistry is an exceptionally precise method to spectroscopic study of electrochemical processes, which simultaneously demonstrates the formation and disappearance of redox species. And it helps to understand the exact mechanism in which these formations and disappearances are taking place.

1-2 Photoelectrochemistry

Photoelectrochemistry studies the interaction between light and electrochemical systems. In another word, it is the reaction on the electrode in an excited state.[10] This excitation can be originated from an electrode (metal or semiconductor) or a substance (adsorbed molecules) at the interface between the electrode and a solution.[10] In photoelectrochemical experiments, irradiation of an electrode with light, absorbed by electrode material, causes the production of a current which is called photocurrent.[3] The dependence of photocurrent on the wavelength, electrode potential, and solution composition provides information about the nature of photoprocesses and their energetic and kinetics.[3] Early work has been done by a French scientist called Becquerel who observed a current flow through the external circuit when two metal electrodes (selected from platinum, gold, silver, and brass) were immersed into acidic, neutral and alkaline electrolytes and one of the electrodes was exposed to sunlight.[10,11] Since his attempts in 1839, more extensive studies have been conducted on photoelectrochemical and electrochemical reactions where electrolyte solution was irradiated. In recent years,

tremendous surge of interest has been developed in the field of photoelectrochemistry, particularly in the application of photoelectrochemical systems to the problem of solar energy conversion and storage.[12] This activity has been stimulated by the public awareness, and concern with, the problem of developing new energy sources to supplement, and eventually replace, fossil fuels.[12] In a historical context, it is interesting to note that most of the studies in the 1970s and the early 1980s were oriented toward the photovoltaic conversion, the conversion of sunlight to electrical power, and energy storage possibilities with photoelectrochemical (PEC) devices. In the late 1980s and with the falling of oil prices a reorientation of PEC studies toward materials synthesis, processing, and characterization particularly with the electronics industry as a target consumer was promoted.[13,14] Simultaneous with this trend was the realization that PEC methods, and specifically photochemistry (PC) techniques, which can play a useful role in hazardous waste treatment.[13,15-27] Until now, photovoltaics has been dominated by solid-state junction devices, often made of silicon. Recently, the emergence of a new generation of photovoltaic cells, based on nanocrystalline materials and conducting polymer films has been the topic of most studies.[28] These cells offer the prospect of cheap fabrication together with other attractive features, such as flexibility. The phenomenal recent progress in fabricating and characterizing nanocrystalline materials has opened up whole new window of opportunity. Surprisingly, some of the new devices have high conversion efficiencies, which compete with those of conventional devices.[28]

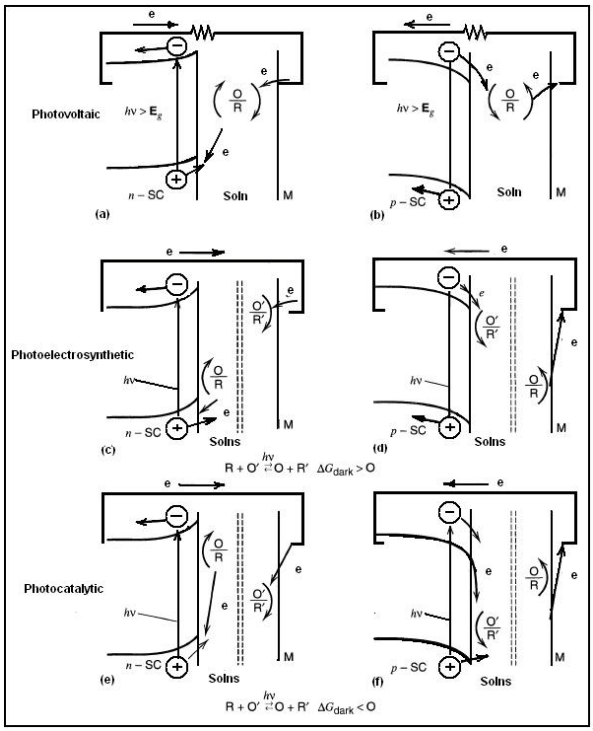

Figure 1-6 Different types of photoelectrochemical cells for p-type (a, c, and e) and n-type (b, d, and f) semiconductors (Reprinted from reference 3).

All phenomena associated with the photoelectrochemical systems are based on the semiconductor-electrolyte interface.[3] There are three types of photoelectrochemical cells including, photovoltaic cells, photoelectrosynthetic cells, and photocatalytic cells.[3] Photovoltaic cell converts light to electricity with no net charge in the solution composition and electrode material. In photoelectrosynthetic cells the net cell reaction is driven by light in the non-spontaneous direction so that the radiant energy is stored as the chemical energy.[3] Photocatalytic cells are similar to photoelectrosynthetic cells except the reaction is driven in a spontaneous direction which normally would be very slow in the dark, so the light energy is being used to overcome the energy of the activation process.[3] The efficiency of last two systems is often low. Schematic illustration of these cells is depicted in Figure 1-6.[3]

The main compartment of every PEC is the semiconductor which converts incident photon to electron-hole pairs.[3] Based on the electrical conductivity, materials are classified into three groups, conductors, insulators, and semiconductors. Semiconductors are substances with the property between insulators and conductors (metals).[3] It is well known that in a solid material, the atoms are compacted, due to so closely spaced orbitals which are essentially present as continuous bands, rather than isolated atoms with individual energy levels. The filled bonding orbitals constitute the valence band (VB) and the vacant antibonding orbitals constitute the conduction band (CB). The gap between the valence and conduction bands is known as the band gap and it is measured in the units of electron volts. A schematic description of the electronic energy structure for solids is shown in below in Figure 1-7.[3] In the case of semiconductors, the band gap is not too large, and the excitation of electrons by required energy causes them to move from the valence band to the conduction band, thereby facilitating conduction of electricity. The excitation could be caused by thermal energy or light energy.[3]

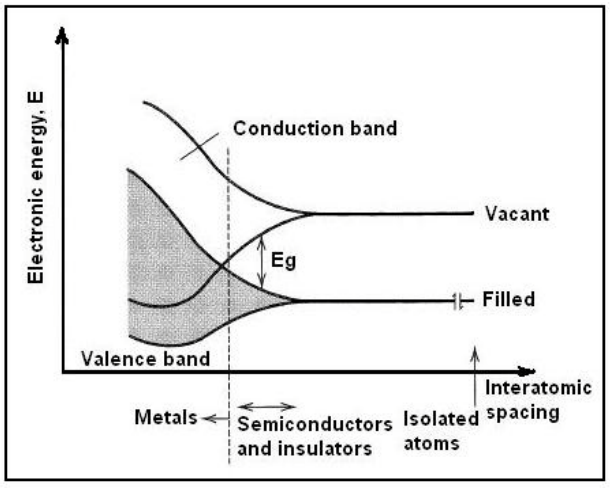

Figure 1-7 Electronic energy structure of solids (Reprinted from reference 3).

1-3 Photoelectrochemical Conversion of CO_2

Global warming[29] is an unusually rapid increase in the temperature of earth's surface for the past few decades and scientists are convinced that greenhouse gases are the origin of this effect which can lead to extreme weather patterns, extinction of animal species, and so on. The reason for this increase in temperature is the phenomenon called greenhouse effect. When solar radiation passes through the atmosphere, about 50% of it is absorbed by the earth's surface and serves to warm our planet so that it becomes habitable; the rest is reflected back by the earth's surface and its atmosphere. This reflected radiation is trapped due to the molecular vibrations and infrared absorption of the greenhouse gases including, water vapor (H_2O), carbon dioxide (CO_2), methane (CH_4), ozone (O_3), chlorofluorocarbon (CFC), and nitrous oxide (NO), and reemitted in all directions, specially back to the earth's surface which leads to an increase in the average temperature of the atmosphere near the earth.[29] One of the biggest contributors to the greenhouse effect is CO_2. Despite being the relatively weak greenhouse gas, so much CO_2 has been emitted in the air that it has the largest effect on the greenhouse effect. The amount of CO_2 has been increased due to burning of fossil fuels in cars, power plants and industry.[30] Thus, the reduction of CO_2 to fuels and organic compounds using light, electricity, or a combination of both, has been the topic of numerous studies since 1800s, although rapid progress was made only since the 1970s.

Figure 1-8 indicates the contribution of CO_2 among greenhouse gases and also the total emissions of CO_2 from fossil fuels in 2011.[30] A major challenge in conversion of CO_2 relates to the fact that its molecule is extremely stable and is kinetically inert.

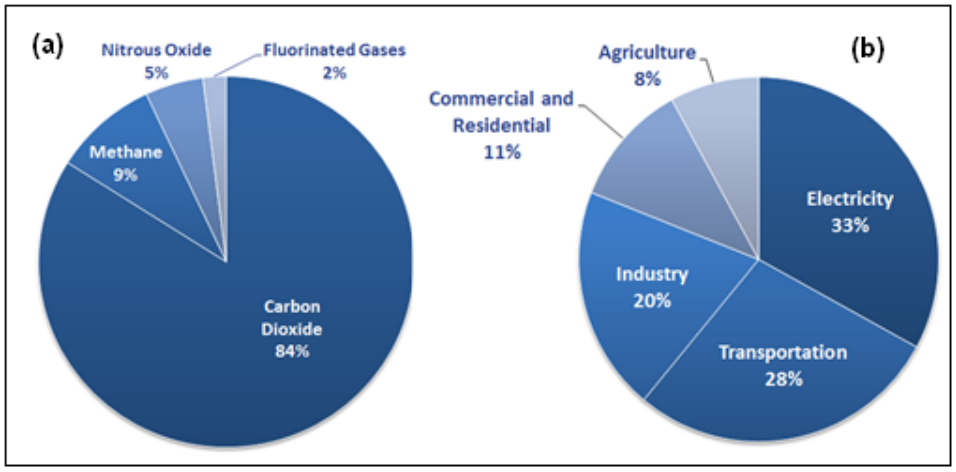

Figure 1-8 Pie chart for the contribution of CO_2 as a greenhouse gas (a) and total emissions of CO_2 due to the burning of fossil fuels (b) (Reprinted from reference 30).

The most common redox reactions that are related to CO2 reduction are as follows[31]:

$$CO_2 + H^+ + 2e^- \longrightarrow HCOO^- \qquad E^0 = -0.61 \text{ V vs. NHE} \qquad (1.4)$$

$$CO_2 + 2H^+ + 2e^- \longrightarrow CO + H_2O \qquad E^0 = -0.53 \text{ V vs. NHE} \qquad (1.5)$$

$$CO_2 + 6H^+ + 6e^- \longrightarrow CH_3OH + H_2O \qquad E^0 = -0.38 \text{ V vs. NHE} \qquad (1.6)$$

$$CO_2 + 8H^+ + 8e^- \longrightarrow CH_4 + 2H_2O \qquad E^0 = -0.24 \text{ V vs. NHE} \qquad (1.7)$$

Several techniques have been developed by scientists to find the best way to reduce carbon dioxide to useful products. For over a century, electrochemical reduction of carbon dioxide has been studied due to its significant impact as a solution for both the energy and environmental issue. Using carbon dioxide as a feedstock is a way to control CO_2 levels in atmosphere. In this method, electricity generated from renewable energy sources such as solar, wind, hydro, nuclear, wave, tides, and geothermal serves as an external power supply for electron transport. With highly efficient electrocatalysts designs, carbon dioxide reduction reaction to valuable compounds and alternative fuels can displace the conventional fuels and ease the world's dependence on fossil fuels.[32]

Electrochemical reduction of CO_2 at solid electrodes yields to different kinds of organic substances like carbon monoxide (CO), methane (CH_4), ethanol (C_2H_5OH) and methanol (CH_3OH).[31] Electrode materials for reduction of CO_2 can be categorized in three different groups.[33] These three groups are differentiated based on two major factors, hydrogen overpotential and CO adsorption on the electrode surface. [33] Overpotential is usually defined as the difference between the potential of an electrode under the passage of current and the thermodynamic value in the absence of electrolysis.[31] Thus, hydrogen overpotential corresponds to a wide window of potential in which the hydrogen production occurs. Adsorption of CO on metal surfaces, known as poisoning electrode surface, is frequently correlated with hydrogen adsorption because both molecules compete for surface sites. The affinity of these species for metal surface depends strongly on the metal itself and may take place in a dissociative fashion, for instance as H_{ads}, hydrogen adatoms, or in a molecular form, H_2. In general, dissociative adsorption is an adsorption with dissociation into two or more fragments which both or all are bound to the surface of the adsorbent. Molecular adsorption indicates a weak interaction between the species, for instance CO of H_2, and the metal surface, and they can be eliminated from the surface by raising the temperature of the metal.[31]

The first group of metal electrodes comprises of those with high hydrogen overpotential and negligible CO adsorption including, mercury (Hg), cadmium (Cd), lead (Pb), indium (In), tin (Sn), and thallium (Tl).[33] The former property enables them to prevent the hydrogen production at positive potentials. Low CO adsorption onto these electrode surfaces relates to the ability of this group to desorb the CO produced in the reaction, in this way avoiding the poisoning effect. Both of these characteristics are positive aspects of using these groups of metals for CO_2 reduction. However, they are poor electrocatalysts in a sense that they cannot break the C-O bond in CO_2 so the main

product of their reaction is either formate or formic acid. Furthermore, they are highly toxic and therefore not environmentally favorable. [33]

The second group consists of low hydrogen overpotential with a strong strength for CO adsorption such as, platinum (Pt), nickel (Ni), iron (Fe), and titanium (Ti).[33] In this group of metals, CO_2 is reduced to form strongly adsorbed CO and this adsorption, which poisons the electrode surface, in turn decreases the electroactive surface area and forces the electrochemical reaction to stop. Although, if the reaction is pushed further by applying more cathodic current, generation of molecular hydrogen turns out to be the main electrochemical product. Therefore, the low hydrogen overpotential property in this group does not let the electrode to go further in the negative potential to reduce CO_2 and leads to hydrogen production as the main product. [33]

The last group comprises of metal electrodes with medium hydrogen overpotential and weak CO adsorption like, gold (Au), silver (Ag), zinc (Zn), and copper (Cu).[33] They can be considered as one of the best group of metals that have the ability to break the C-O bond and reduce carbon dioxide to CO with a high current efficiency. Among these metals, only copper can reduce CO to hydrocarbons. [31]

Therefore, copper electrodes are considered as the most promising candidates for the hydrocarbon production. Copper electrodes have been used in different manners such as, Cu-alloys, Cu-coated metallic electrodes, Cu based composites, and Cu modified with other transition metals.[31] Thorough investigation for electroreduction of CO_2 to hydrocarbons has been reported by Hori and his group on copper foil electrodes.[34,35] The effect of aqueous[36-45] and non-aqueous[46-54] electrolytes on the faradaic efficiency and distribution of product have been studied using metallic copper electrodes or mixture of that with other transition metals for CO_2 electroreduction. Electrocatalytic activities of

copper electrodes for CO_2 reduction have also been reported.[54-58] Electroreduction of CO_2 using copper electrodes is summarized in Table 1.1.[31]

Table 1-1 Trends in carbon dioxide electroreduction from 1998-2005.

Year	Electrode material	Experiments parameters	Main products	Refs
1998	Cu-Zn	Electroreduction at -1.30 V	C_2H_4, C_3H_7OH	42
1999	Cu	Aqueous media	CH_4, C_2H_4	49
	Cu	CSOH/Methanol	CH_4, C_2H_4, H_2	50
2002	Cu	Aqueous $NaHCO_3$	CH_4	38
	Cu-Rh, Cu-Ru	Method: EQCM with CV	CO, CH_4	39
2004	Cu mesh	Neutral solution	C_2H_4, H_2	47
2005	Cu	Deactivation of Cu	CH_4	31
	Cu-Au	0.1 M $KHCO_3$ and K_2SO_4	CH_4, C_2H_4	40

However, the multielectron ($6e^-$) transfer for the conversion of CO_2 to methanol has not been reported in most of these works. The reasons for that are the high amount of energy needed for this conversion and also the deactivation phenomena that these groups of metals are suffered usually 20-30 minutes after the start of electrolysis which greatly depends on the chemical reagent that has been used.[31] Herein, another step was taken through a better and more efficient way to use copper electrodes for CO_2 electroreduction. In addition, one of the best ways to address the issue of required high energy for the conversion is to consider solar energy as the driving force. Unfortunately, metallic copper electrodes are inactive under the passage of light. Thus, the most effective way to take advantage of solar energy with copper electrodes is the utilization of their oxides, which are semiconductors and therefore can be used as an electrode material for photoelectroreduction of CO_2. Given that CO_2 is a greenhouse gas, using

sunlight to convert CO_2 to transportation fuel, such as methanol, represents a value-added approach to the simultaneous generation of alternative fuels and environmental remediation of carbon emissions from the continued use of conventional fuels.

Copper oxide has two different metal oxidation states, cuprous oxide (Cu_2O) and cupric oxide (CuO); these two compounds have energy band-gaps of ~ 2.0-2.2 eV and 1.3-1.6 eV, respectively.[59] Additionally both oxides have high absorption coefficients over a substantial portion of the solar spectrum, as shown in Figure 1-9.[60]

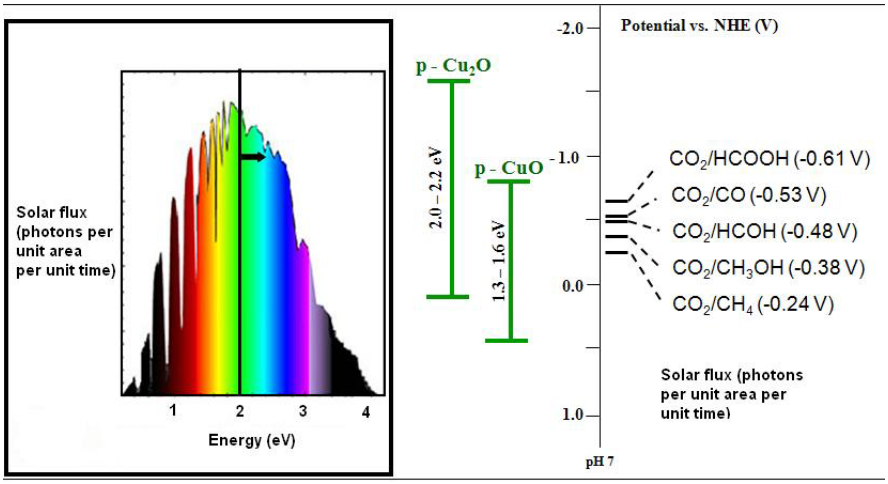

Figure 1-9 Spectral distribution of solar photon flux and the band position of copper oxide semiconductor (Reprinted from reference 60).

Importantly, from a sustainability and toxicity perspective, the component elements are plentiful and relatively less toxic in comparison to other elements such as Cadmium (Cd) or Arsenic (As), which are present in other compound semiconductors like Gallium Arsenide (GaAs) and Cadmium Telluride (CdTe).[61-63] The position of conduction band edge lies at very negative potentials, relative to other oxides such as titanium oxide (TiO_2)[34] and tungsten oxide (WO_3)[64], translating to high reducing power for the photogenerated electrons.[32] Semiconductor colloids such as Cadmium Sulfide (CdS) and

Zinc Sulfide (ZnS) have been used by other authors for the photocatalytic reduction of CO_2. The products in these cases are mostly formate and/or formaldehyde.[65] Two-electron reduction products such as CO and formic acid have been reported in some cases in place of the (more difficult) six-electron conversion to methanol.These photoelectrons have been employed for the photogeneration of H_2 from water using both Cu_2O and CuO. Also, both of these oxides were demonstrated to afford high photocurrent densities for water reduction to hydrogen. Despite high electrocatalytic activity of copper and its oxides for CO_2 reduction there were no reports for the use of copper oxides for the photoreduction of CO_2. Thus, the inspiration for using copper/copper oxides photoelectrodes in this thesis originated from the Cu catalytic properties and the excellent matching of the Copper oxide band gaps with the energy of the solar light.

The crystal structures of these photoactive oxides together with the Cu structure are shown in Figure 1-10. [66]

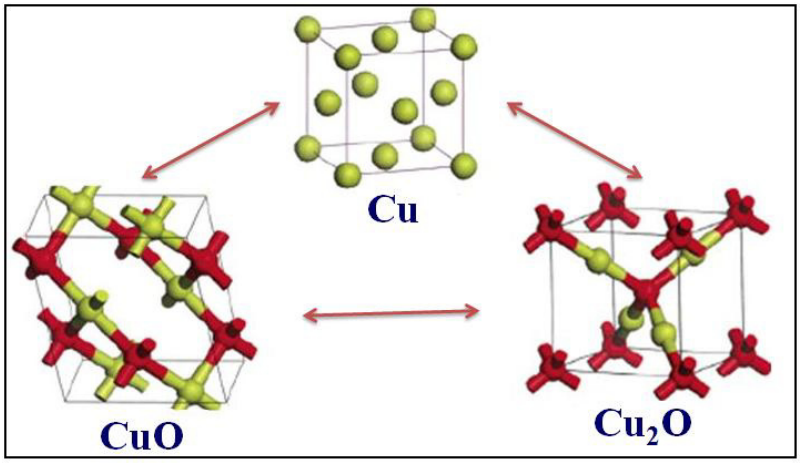

Figure 1-10 Crystal structures of copper and its oxides (Reprinted from reference 66).

Selective conversion of CO_2 to methanol has several redeeming features especially in light of the fact that large amounts of this chemical are manufactured world-

wide. For example, in the U.S. alone there are eighteen methanol production plants with a cumulative annual capacity of over 2.6 billion gallons.[67,68] However, the current feedstock for this production is hydrocarbon-based with a sizeable carbon footprint. Further, the high operating pressures and temperatures needed for steam reforming translates to correspondingly high capital investment and a long energy pay-back period. Therefore mild methods for producing methanol from environmentally problematic feedstocks such as CO_2 take on added importance.[32]

One limitation for using Cu_2O as a photoelectrode is its poor stability in aqueous electrolytes because the redox potential for Cu_2O/Cu^0 is located within the band gap of the semiconductor. The performance/stability of Cu_2O photoelectrodes can be however enhanced by metal and/or semiconductor coatings[64,69] as well as solution electron shuttles such as methyl viologen.[64] For instance, the stabilization of electrodeposited Cu_2O photoelectrodes by a nickel (Ni) surface protection layer and the use of an electron shuttle in solution has been reported.[64] Also, enhanced photoactivity of electrodeposited Cu_2O was recently reported under a surface protection consisting of Al-doped ZnO and TiO_2 nanolayers to avoid photocathodic decomposition.[69] These films were also activated with Pt nanoparticles to enhance solar hydrogen generation.[69] Photocurrents for electrodeposited Cu_2O were separately optimized for solar H_2 generation without using any surface treatment.[70]

While recent attempts have been focused in protecting layers,[64,69] metal and/or semiconductor on Cu_2O photocathodes in order to move out the photogenerated minority carriers, electrons, and thus avoiding Cu_2O photocorrosion to Cu^0, none has intended to use hierarchical CuO/Cu_2O (core/shell) nanorod heterostructures. The importance of using nanostructured photoelectrodes is mainly to enhance the separation of photogenerated electrons and holes in the structure of these oxide semiconductors. First,

by transporting Cu_2O photoelectrons toward the CuO inner wire and second, by increasing charge separation, holes to Cu_2O and electrons to CuO, thus enhancing charge transfer to the electrolyte.

In this dissertation, solar photoelectrochemical reduction of carbon dioxide to methanol in aqueous media is investigated on hybrid CuO/Cu_2O semiconductor nanorod arrays for the first time at potentials ca. 800 mV below the thermodynamic threshold value and at Faradaic efficiencies of ca. 95%.[62] The CuO/Cu_2O nanorod arrays were prepared on Cu substrates by a two-step approach consisting of the initial thermal growth of CuO nanorods followed by controlled electrodeposition of p-type Cu_2O crystallites on their walls.[62] The resulting nanorod morphology with controllable wall thickness by adjusting the Cu_2O electrodeposition time as well as their surface/bulk chemical composition were probed by scanning electron microscopy, X-ray diffraction and Raman spectroscopy. Photosynthesis of methanol from carbon dioxide was demonstrated at -0.2 V vs. standard hydrogen electrode (SHE) under simulated air mass (AM) 1.5 solar irradiation on optimized hybrid CuO/Cu_2O nanorod electrodes and without addition of any homogeneous co-catalysts, such as pyridine, imidazole or metal cyclam complexes, were used contrasting with earlier studies on this topic using p-type semiconductor photocathodes. The roles of the core/shell nanorod electrode geometry and the copper oxide composition were established by varying the time of electrodeposition of the Cu_2O phase on the CuO nanorod core surface. The hybrid composition ensuring double pathway for photoelectron injection to CO_2 along with high surface area was found to be crucial for efficient performance in methanol generation under solar illumination.[32]

1-4 Electrochemical Study of Flavins

The yellow-colored compounds with the basic structure of 7,8-dimethyl-10-alkylisoalloxazine are generally termed as flavins.[71] flavins are unique compounds in nature which take part in many biochemical reactions as coenzymes and photoreceptors.

Riboflavin, the precursor of all the biologically important flavins, was first reported as lactochrome, a bright yellow pigment isolated from cow milk in 1879.[72] Majority of flavins are existed as flavocoenzymes, mainly as flavin adenine dinucleotide (FAD), and in lesser amounts as flavin mononucleotide (FMN). Structures of all three compounds are illustrated in Figure 1-11.[71] chemical reactions of flavins undergo reversible redox conversion. Redox properties of these compounds were investigated by many authors using polarography and potentiometry techniques.[71] Flavins have been recognized by their ability of participate in both one- and two-electron transfer processes.[73]

This means that flavin molecules can exist in three different redox state, the fully oxidized flavoquinone (Fl_{ox}), the flavosemiquinone radical in either the anionic ($Fl_{rad}^{\cdot -}$) or neutral ($Fl_{rad}H$) form and the two electron reduced flavohydroquinone either anionic ($Fl_{red}H^-$) or neutral ($Fl_{red}H_2$) form.[73]

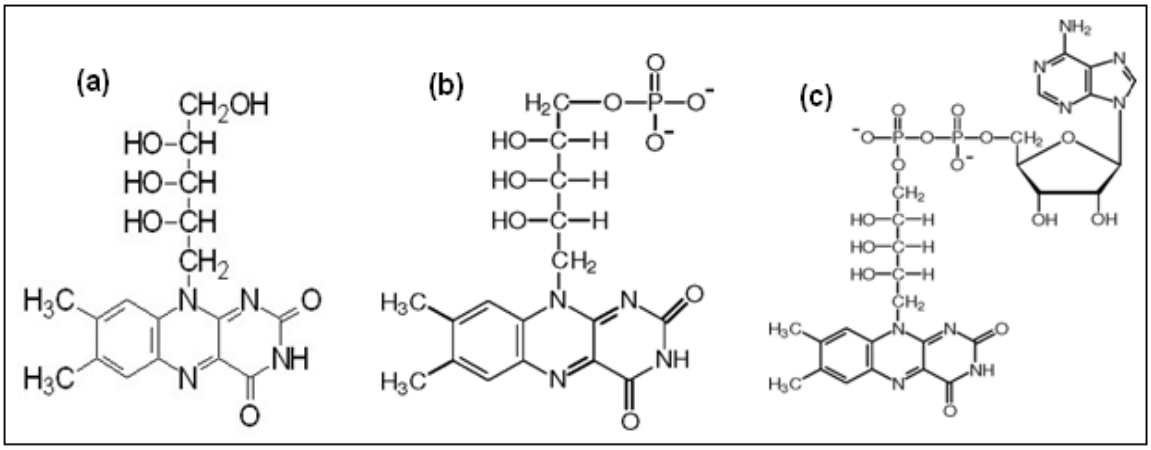

Figure 1-11 Chemical structure of (a) riboflavin (RF), (b) flavin adenine dinucleotide (FAD) and (c) flavin adenine mononucleotide (FMN) (Reprinted from reference 71).

The redox equilibrium of flavins in aqueous media is pH dependent and it involves up to two electrons and two protons. Two regions are distinguished in the plot of pH versus formal potential with two different slopes suggesting the change in the number of protons in the process.[73] For a couple where Ox is the oxidized species and Red, is the reduced species,[74]

$$Ox + ne^- + mH^+ \rightarrow Red^- H_m^{(m-n)+} \quad (1.8)$$

$E_{1/2}$ decreases with pH as 0.05916 (m/n), where *m* and *n* are the numbers of transferred protons and electrons, respectively. This equation which is based on the Nernst equation shows that the redox reaction involves two electron and two protons resulting a slope of 66 mV per unit pH in acidic media. While in basic media, the slope corresponds to two electron and one proton process with the value of 33 mV per unit pH.[74]

The redox properties of flavins have been studied since 1900 and it is well known that the fully oxidized flavoquinone is immediately reduced to flavohydroquinone in a two-electron and two-proton process.[73] The electrocatalytic role of flavin adenine dinucleotide (FAD) in the electroreduction of some biological molecules including, cytochrome, glucose oxidase, methemoglobin, and the electrooxidation of ferredoxin on a Pt electrode has been demonstrated by Durliat et al.[75] A new method for surface reconstitution of apo-flavoenzymes by the assembly of a relay-FAD monolayer on the gold (Au) electrode has also been developed.[76] Kumar and Chen have modified a glassy carbon electrode (GCE) with a poly (*p*-aminobenzenesulfonic acid) (PABS)/FAD film for detection of nicotinamide adenine dinucleotide.[77] The electrocatalytic oxidation and reduction of NADH and NAD^+, respectively, using a GCE modified with a nordihydroguaiaretic acid (NDGA)/FAD hybrid film have been performed by Chen and Liu.[78] Lin and Chen have developed a FAD/zinc oxide-modified GCE to increase the electrocatalytic reduction current of O_2, H_2O_2, CCl_3COOH, and SO_3^{2-} in the presence of hemoglobin.[79]

The electrochemical behavior of flavins in solutions and on modified electrode surfaces has been extensively investigated using various electrochemical techniques including, polarography, chronopotentiometry, cyclic voltammetry, AC voltammetry, scanning tunneling microscopy, and quartz crystal microbalance.[80-90] Birss et al. has shown that FAD adsorbs very strongly in three different orientations on Hg electrode surface.[83,84] McGarvey et al. also has studied the orientation of FAD adsorbed on Hg electrode.[85] Kubota et al. has demonstrated that FAD can be strongly immobilized on TiO_2-modified carbon fibers, and remains stable for at least two months.[86] Wang et al. has shown that FAD weakly adsorbs on gold when it is present at low concentration in a solution.[87] Gorton and Johnasson have found that FAD strongly adsorbs on graphite, and that the FAD-covered graphite electrode remains very stable even after being exposed to air for more than two months.[88] On the other hand, the adsorption of FAD on a GCE was very weak, and the adsorbed FAD layer was easily removed off the electrode surface by washing. The same two observations were reported by Miyawaki and Wingard.[89,90] However, the same authors also have shown that a stable FAD layer could be formed on a GCE, if the molecule is covalently attached to the surface, which was achieved by electrochemical activation of glassy carbon.[90] Recently, a number of proton-coupled electron transferred (PCET) reactions have been examined in considerable details, and examples have been reported which occur via concerted, where the electron and proton transfer simultaneously, and consecutively, where the electron and proton transfer separately, mechanisms.[73,91] Unique versatility allows flavins to act as intermediaries between compounds that donate two electrons (e.g., NADH, succinate) and compounds that only accept one electron at a time (e.g., heme Fe). Their unique reactivity with oxygen also enables flavins to take part in important aerobic processes.[91]

This dissertation presents the speciation and mechanistic details of the electroreduction and protonation of the newly synthesized, 1, 3-diamine flavin, thereafter denoted as Fl^{2+}. This compound is formed by the tricyclic heteronuclear organic ring, isoalloxazine (shown in Figure 1-12b), possessing two amine groups in the N (1) and N (3) positions as shown in Figure 1-12a. The water soluble cation, in aqueous electrolytes adjusted to selected pHs in the range from 1 to 10 using a bare GCE as the working electrode. This compound, Fl^{2+}, shows only one cathodic redox process, determined to be a two-electron process involving either one- or two-proton depending on the pH.

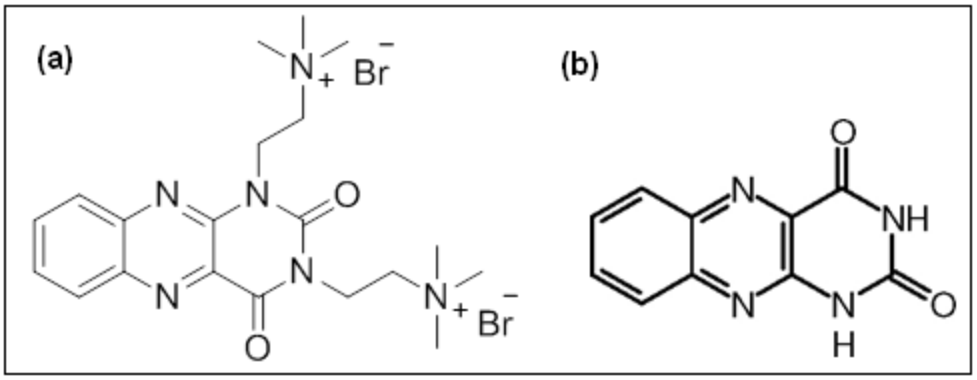

Figure 1-12 Molecular structure of (a) 1, 3 - diamine flavin and (b) isoalloxazine.

Spectroelectrochemistry, performed in integral and differential modes, was used to determine the mechanistic details of this electroreduction process. It is worth to note that this compound demonstrates a potential electrocatalytic reduction of oxygen. Therefore, a brief study on the electrocatalytic activity of the compound for oxygen reduction will be also discussed. Also, electrochemical behavior of the compound using gold and copper/copper oxide as working electrodes is investigated. Finally, the effect of saturation with CO_2 gas on the behavior of the compound will be examined.

Chapter 2

Tailoring Copper Oxide Semiconductor Nanorod Arrays for Photoelectrochemical Reduction of Carbon Dioxide to Methanol

Solar photoelectrochemical reduction of carbon dioxide to methanol in aqueous media was driven on hybrid cupric/cuprous oxide (CuO/Cu_2O) semiconductor nanorod arrays for the first time. A two-step synthesis was designed and demonstrated for the preparation of these hybrid one-dimensional nanostructures of copper oxide on copper substrates. The first step was consisted of the growth of CuO nanorods by thermal oxidation of a copper foil at 400 °C. In the second step, a controlled electrodeposition of p-type Cu_2O crystallites on the CuO walls was performed. The resulting nanorod morphology with controllable wall thickness by adjusting the Cu_2O electrodeposition time as well as their surface/bulk chemical composition were probed by scanning electron microscopy, energy dispersive X-ray analysis, X-ray diffraction and Raman spectroscopy. Photoelectrosynthesis of methanol from carbon dioxide was demonstrated at -0.2 V vs. SHE under simulated solar irradiation on optimized hybrid CuO/Cu_2O nanorod arrays electrodes and without assistance of any homogeneous catalyst (such as pyridine or imidazole) in the electrolyte. Morphology and composition of the hybrid CuO/Cu_2O photoelectrodes were found to be crucial for efficient performance in methanol generation under solar illumination. Methanol formation, tracked by gas chromatography equipped with mass spectrometer, indicated Faradaic efficiencies of up to 95%.[32,92]

2-1 Experimental

2-1-1 Chemicals and Methodology

Copper (Cu) substrates, foil and mesh, were from Alfa Aldrich and 99.99% purity. Chemical reagents used in the study were of analytical grade and were used without further purification. For preparation of the copper oxide electrodes three main methods

were utilized including, anodization,[93] cathodic electrodeposition,[94-99] and thermal oxidation[100,101] on different substrates (such as, copper mesh, foil). Prior to each experiment, a pretreatment process was carried out for each substrate, consisted of three consecutive washings performed by 5 min sonication with isopropanol, acetone, and deionized water and then drying the films under nitrogen (N_2) gas. All potentials were measured vs. Ag/AgCl reference electrode but they are quoted with respect to SHE, using Ag/AgCl = -0.197 V vs. SHE.

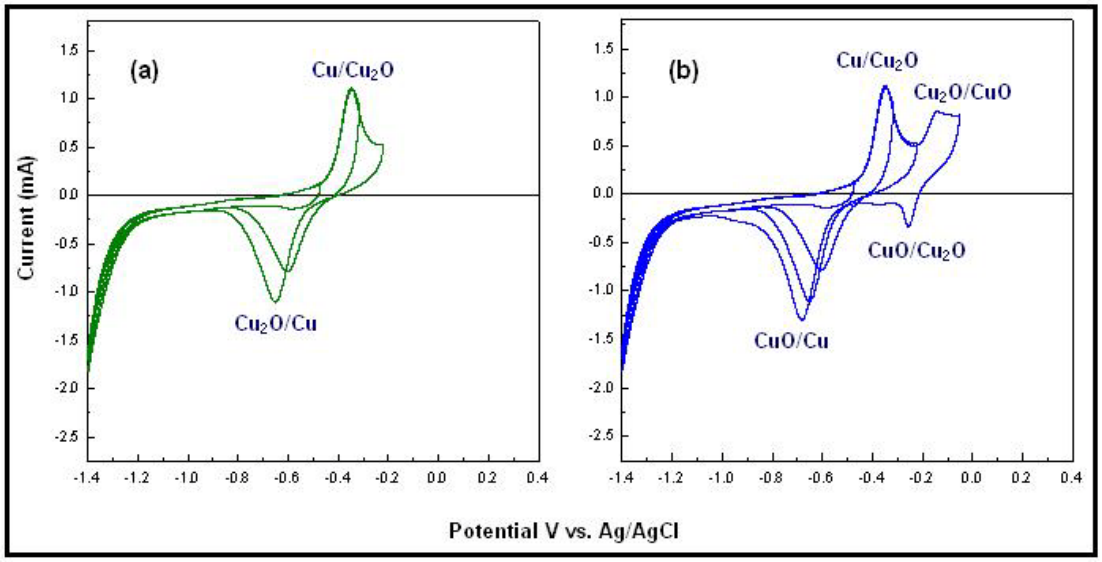

Figure 2-1 Cyclic voltammograms of a copper mesh in 0.1 M NaOH. The scans were initiated at -1.4 V and in the positive direction, using different potential windows to distinguish the formation and electroreduction of Cu_2O (a) and CuO (b) respectively using a potential scan rate of 0.05 V/s.

Electrochemical oxidation (anodization) was performed on the copper foil electrodes in a solution containing 0.1 M sodium hydroxide[93] (NaOH) to determine the optimal potential window for the formation of the copper oxides. For this experiment the copper foil was immersed in 0.1 M NaOH solution and then cyclic voltammetry was

performed from -1.4 to 0.0 V vs. Ag/AgCl (-1.2 to 0.2 V vs. SHE) at the scan rate of 0.05 V/s. Suitable potential range was found to be -0.35 to -0.65 V vs. Ag/AgCl (sat. KCl), -0.15 to -0.45 V vs. SHE, as is displayed in Figure 2-1. Formation of CuO occurs at potentials higher than -0.2 V vs. SHE versus Cu_2O, Figure 2-1b. The best potential for the formation of the Cu_2O was found to be -0.2 V vs. SHE.

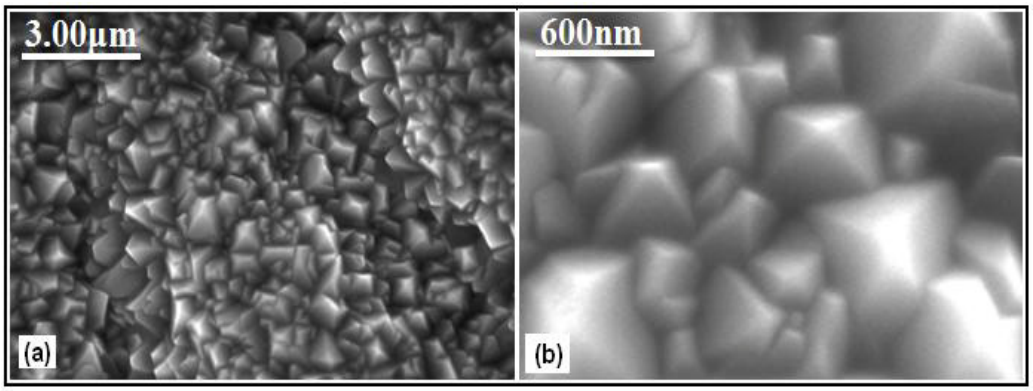

Figure 2-2 SEM images of a Cu_2O film grown by cathodic electrodeposition at -0.4 V vs. Ag/AgCl in an aqueous solution containing 0.4 M $CuSO_4$ 3 M lactic acid at pH 9. SEM magnifications are x10.0K and x50.0K for (a) and (b) respectively.

Potentiostatic electrodeposition of cuprous oxide (Cu_2O) films consisted of using a constant potential of -0.2 V vs. SHE from a lactate-stabilized cupric sulfate ($CuSO_4$) solution of pH 9 following a reported procedure by Switzer et al.[96,97] The electrolytic bath was prepared with deionized (DI) water (Corning Megapure) and contained 0.4 M $CuSO_4$ and 3 M lactic acid. The bath pH was adjusted to 9 by an addition of concentrated NaOH solution; the temperature of the bath was maintained at 60^0C during the electrodeposition. Film formation occurs by the electroreduction of Cu^{2+} to Cu^+ which is followed by slow precipitation of Cu_2O on the electrode surface. The electrolyte solution was basic in pH to stimulate the formation of Cu_2O and it was also highly concentrated in lactate to stabilize the Cu^{2+} cation, thus avoiding formation of copper hydroxide

$[Cu(OH)_2]$ in solution. Platinum foil and Ag/AgCl (satd. KCl) were used as the counter electrode and reference electrode, respectively. Representative scanning electron microscope (SEM) images of the resulting films are shown in Figure 2-2 in which is clearly discernible the cubical structure of the Cu_2O in two different magnifications.

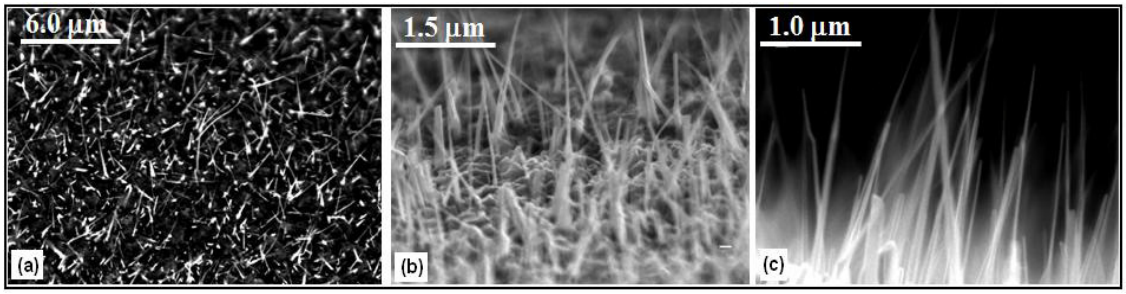

Figure 2-3 SEM images of Cu_xO_y nanowires grown isothermally (400^0C) on a Cu substrate. Magnification scale for (a): x5.0K, (b): x18.0K, (c): x30.0K.

To prepare the thermally oxidized film, freshly cleaned Cu substrates were subjected to thermal oxidation in presence of air using a box furnace for 4 h at 400°C. A temperature program was used and consisted of first heating the sample up to 400°C (at 25°C/min). After 4 h of isothermal heating, the sample was allowed to return naturally to room temperature. The resulting film morphology which consists of standing nanorods is presented in Figure 2-3 at different magnifications. The chemical composition of these thermal grown nanorods is mostly CuO as identified by Raman spectroscopy.

2-1-2 Preparation of CuO/Cu_2O Nanorod Photoelectrodes

The hybrid CuO/Cu_2O nanorod arrays were fabricated by a two-step process performed on freshly cleaned copper foil. Thus, copper foil substrates were pretreated as it was mentioned above. In the first step, thermal oxidation was carried out as it was discussed before and then, Cu_2O crystallites were electrodeposited on the thermally grown CuO nanorods from a basic solution of lactate-stabilized copper sulfate using a

potentiostat (CH electrochemical workstation 720C). A Pt foil and an Ag/AgCl (satd. KCl) were used as counter electrode and reference electrode respectively. The electrodeposition time was varied to investigate the structural attributes, and also the photoactivity of the resulting heterostructures.

2-1-3 Measurement of Photoelectrochemical Activity

The photocurrent-potential profiles were recorded under solar irradiation (AM1.5) from a solar simulator (Newport 91160-1000). The radiation was interrupted (with a manual chopper) at 0.2 Hz. Bulk photoelectrolysis was also performed in a two-compartment sealed electrochemical cell under continuous light irradiation. The electrolyte used was 0.1 M Na_2SO_4, the solution was saturated with N_2 and CO_2 bubbling through the cell. The CH electrochemical workstation 600C was used to apply a constant potential of -0.2 V vs. SHE. Light irradiation (AM 1.5) was provided by the full output of the Newport solar simulator specified and with illumination power of 70 mW cm^{-2}.

Long term photoelectrolysis was carried out using a CH electrochemical workstation 600C instrument (www.chinstruments.com), in a custom-designed two-compartment, three-electrode electrochemical cell. Ag/AgCl (satd. KCl) and Pt foil were used as reference electrode and counter electrode respectively although all potentials are quoted with respect to the SHE reference scale. The electrolytes used were 0.1 M $NaHCO_3$ (saturated with CO_2) and 0.1 M Na_2SO_4 (saturated with N_2) as control experiment.

2-1-4 Physical Characterization

The surface morphology of the various film samples was characterized using a Hitachi S-5000H field emission scanning electron microscope (SEM) operated at an acceleration voltage of 20.0 kV. Raman spectra were recorded with a HORIBA Jobin Yvon LabRam ARAMIS instrument (incident power $\leq$ 300 mW) using an excitation

wavelength of 532 nm and an 1800 line/mm grating. In all the cases the slit width was 10 μm, and 32 scans were accumulated for each spectrum. X-ray diffraction (XRD) patterns were obtained on a Siemens D-500 powder diffractometer using CuK_{α} as the source radiation.

2-1-5 Gas Chromatography with Mass Spectrometry Detection

Liquid aliquots were periodically taken during the photoelectrolysis to be analyzed in a gas chromatograph equipped with a mass spectrometer as detector (GC-MS). The aliquots were subjected to supporting electrolyte removal by shaking overnight with Amberlite IRN-150 ion-exchange resin (cleaned and vacuum dried just before use) and then injected into the Shimadzu GC-MS 2010SE chromatograph coupled with a MS QP2010 detector and a AOC-20S sampler. Head space sampling was also used for GC-MS analyses to confirm the photoelectrosynthesis of methanol from CO_2 by heating the sealed vial at 75 ºC water bath for 45 minutes to let the liquid and volatile organics equilibrate. The chromatographic column was Shimadzu SHRX105MS (30-m length and 0.25-mm inner diameter, part # 220-94764-02) set at 45 °C. The MS detector was set at 250 °C, and helium was used as the carrier gas. Calibration curves for different methanol concentrations in water showed that the methanol peak eluded at 1.53 min with a corresponding m/z = 31.

2-2 Preparation and Physical Characterization of Hybrid Nanorods

A schematic representation of the preparation of hybrid CuO/Cu_2O photocathodes is shown in Figure 2-4. The first step consists of the formation of CuO nanorod arrays obtained by a thermal procedure.[100] The second step is the cathodic electrodeposition of Cu_2O[98,99] on CuO nanorod arrays at –0.2 V vs. SHE for pre-selected time periods. The resulting photoelectrode samples are designated as TH for the thermally grown CuO nanorods, and TH/EDτ for the CuO/Cu_2O hybrid samples prepared

by electrodeposition for τ min (τ spanning the range: 1-30 min) on the CuO nanorod surface. Table 2.1 provides the nomenclature used to identify the different CuO/Cu_2O nanorod arrays and their respective preparation conditions. Representative SEM images of the resulting CuO/Cu_2O hybrid samples prepared with different electrodeposition time τ are shown in Figure 2-5a-c. Corresponding images for the thermally grown free-standing CuO nanorods (designated as "TH") are presented in Figure 2-5d, while the morphology of an electrodeposited Cu_2O sample on a polished Cu substrate ("ED") is given in Figure 2.5e for comparison. The average nanorod diameter is in the range: 0.8-1.0 μm for TH/ED10 and 1.5-2.0 μm for TH/ED30.

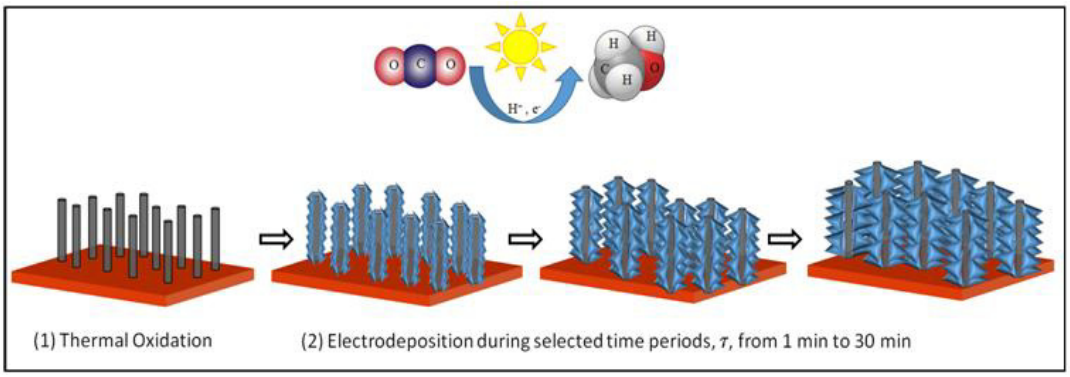

Figure 2-4 Schematic illustration of the two-step synthesis of CuO/Cu_2O hybrid nanorod arrays for solar photoelectrosynthesis of CH_3OH from CO_2: (1) thermal growth of CuO nanorods on a Cu foil and (2) cathodic electrodeposition of Cu_2O for selected times.

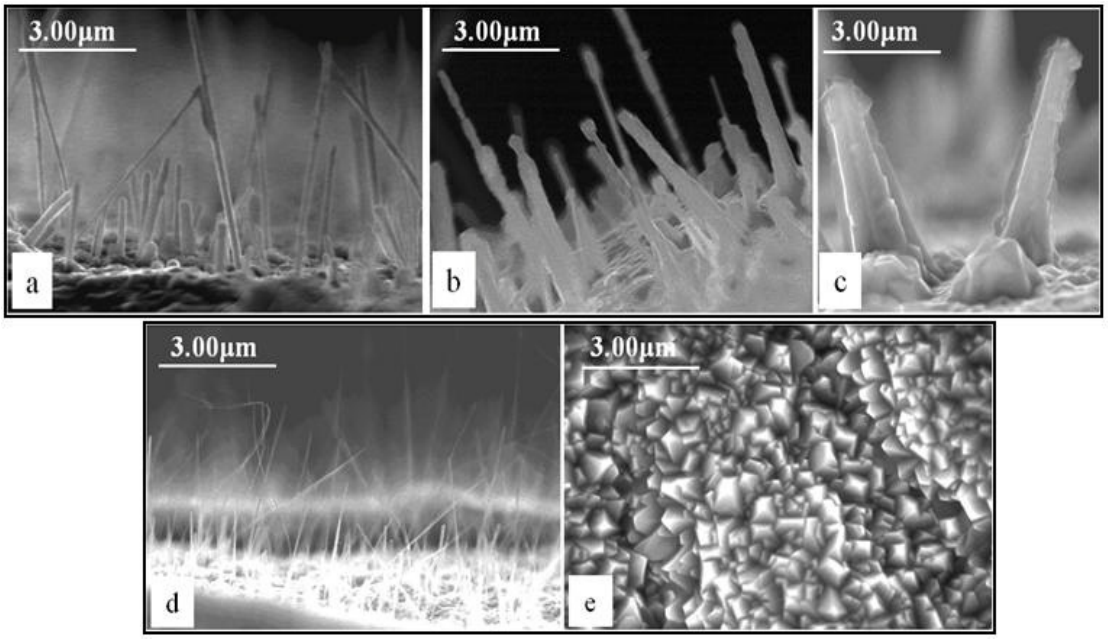

Figure 2-5 SEM images of CuO/Cu_2O hybrid nanorods arrays obtained by a Cu_2O electrodeposition coating on thermally grown CuO nanorods for 1 (a), 10 (b) and 30 min (c) respectively. Thermally grown CuO nanorods (indicated as TH) were used as substrate for the preparation of the respective hybrids (d). Electrodeposited Cu_2O (indicated as ED) on Cu foil without a pre-thermal treatment is included for comparison (e).

The electrodeposition of Cu_2O on the Cu substrate without and with previous thermal growth of CuO nanorods shows a remarkable difference in the resulting amount of Cu_2O electrochemically formed (Figure 2-6). When the CuO nanorods are thermally pre-formed underneath, much more Cu_2O is seen to be electrodeposited (Figure 2-6). This trend is attributable to the much larger surface area of the nanorod array electrode relative to that of a polished Cu substrate. Thus Figure 2-6 compares the charge evolution associated with Cu_2O electrodeposition (τ = 30 min) on the two contrasting substrates: nanorods vs. a flat surface. Note that the electrodeposition charge varies

almost linearly with time for both substrates. The morphology of the resulting films is shown in Figure 2-5c and 5e, and a schematic representation of the two resulting films is included also in Figure 2-6. The large area associated with the CuO nanorods provides a surface aspect ratio enhancement factor of 7-8. This morphological factor will be seen to play a key role in the performance of the Cu_2O/CuO nanorod array photoelectrodes.

Table 2-1 CuO/Cu_2O nanorod photoelectrodes prepared by a two-step strategy (TH and ED) along with the respective parent materials.

Photoelectrode	1^{st} step = thermal (TH)	2^{nd} step = Cu_2O electrodeposition (ED)
TH/ED1	Cu foil heated at 400C, 4 h	Cu_2O electrodeposited for 1 min
TH/ED5	Cu foil heated at 400C, 4 h	Cu_2O electrodeposited for 5 min
TH/ED10	Cu foil heated at 400C, 4 h	Cu_2O electrodeposited for 10 min
TH/ED15	Cu foil heated at 400C, 4 h	Cu_2O electrodeposited for 15 min
TH/ED25	Cu foil heated at 400C, 4 h	Cu_2O electrodeposited for 25 min
TH/ED30	Cu foil heated at 400C, 4 h	Cu_2O electrodeposited for 30 min
TH	Cu foil heated at 400C, 4 h	N/A
ED30	N/A	Cu_2O electrodeposited for 30 min

The data in Figure 2-6 clearly indicate that Cu_2O is able to be continuously electrodeposited on the TH film in spite of its semiconductor nature (i.e., CuO is a p-type semiconductor). It is worth recalling that the electrodeposition mechanism of Cu_2O has been reported to hinge on the presence of surface states in the Cu_2O band gap. These surface states are presumed to mediate hole transfer from the Cu(II) lactate complex to the Cu_2O valence band.[98,99] As the CuO nanorods are vertically situated on a dense film of Cu_2O, it can be speculated that electrodeposition on the nanorod surface is initiated

bottom-up on the dense Cu_2O layer formed thermally.[100] It subsequently advances by progressive upward creep on the CuO nanorods. Evidence may be found in Figure 2-5 where the diameter of the CuO/Cu_2O nanorods is seen to decrease from bottom to top, consistent with a bottom-up growth mode.

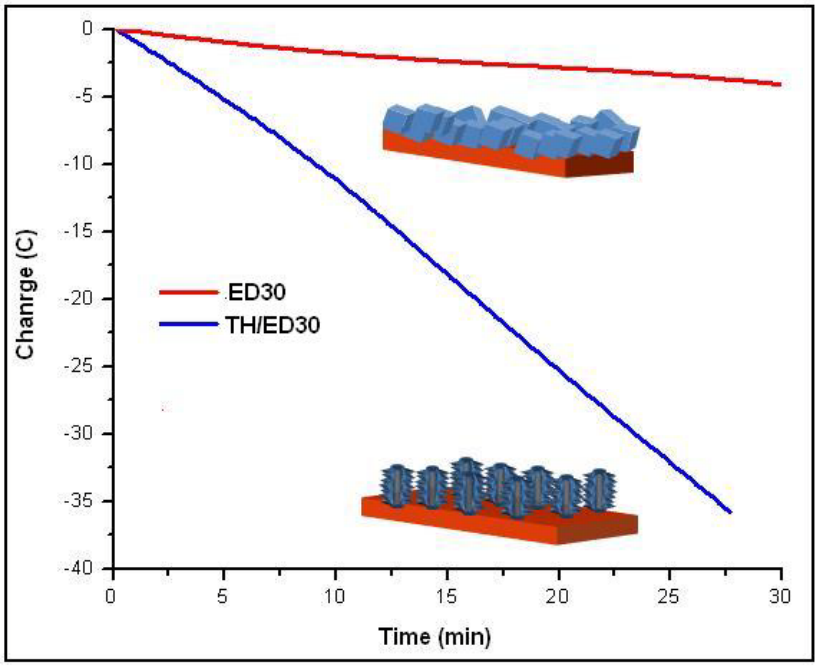

Figure 2-6 Charge evolution during 30 min electrodeposition of Cu_2O on freshly polished Cu foil (ED30) and on thermally oxidized Cu foil (TH/ED30) at -0.20 V vs. SHE using a solution containing 0.4 M $CuSO_4$ and 3 M lactic acid adjusted to pH 9. Color sketches are included to clarify the two contrasting substrates over which the Cu_2O electrodeposition was performed.

XRD and Raman characterization of selected copper oxide films are shown in Figures 2-7 and 2-8 respectively. Comparison of the XRD patterns for TH, ED30 and TH/ED30 samples is provided in Figure 2-7. The JCPDS reference patterns for CuO (80-1917), Cu_2O (78-2076) and Cu (04-0836) are also provided in the figure.

The thermal film (Figure 2-7a) is seen to show the underneath Cu substrate as well as CuO and Cu_2O phases. In fact, the pattern is consistent with a dense Cu_2O film topped with CuO nanorods. During thermal oxidation, a dense Cu_2O surface layer is presumably formed first on the Cu foil. It is then oxidized to CuO leading to a compressive stress that drives outward the diffusion of copper cations along the grain boundaries thus resulting in CuO nanorod formation. The XRD pattern of an ED30 film shows contributions from Cu_2O on the Cu substrate as expected (Figure 2-7b) while the TH/ED30 presents three components, Cu_2O, CuO and Cu, although now the Cu_2O phase makes a larger contribution than in the TH film case (Figure 2-7c).

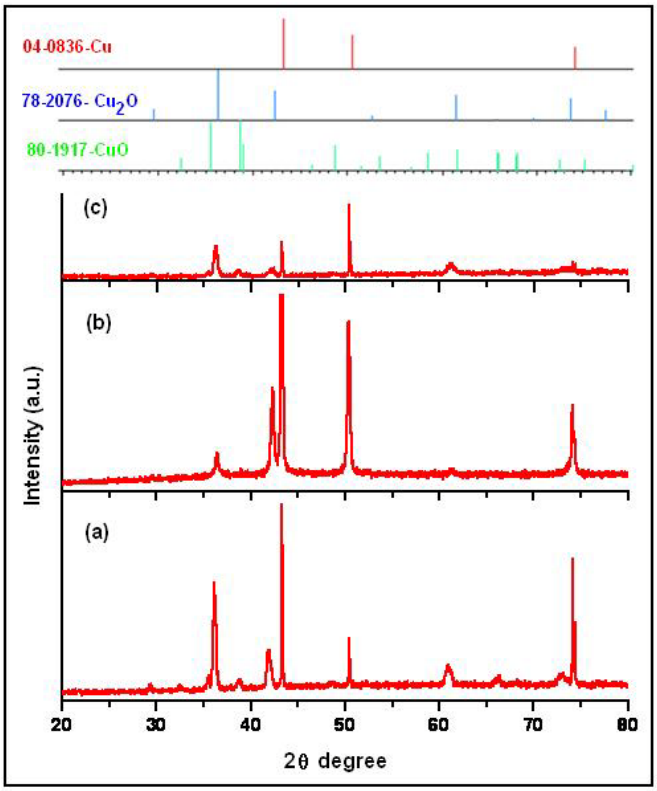

Figure 2-7 XRD spectra of a thermally oxidized (TH, (a)), an electrochemically deposited (ED30, (b)) and a hybrid film (TH/ED30, (c)). Reference JCPDS patterns for Cu, Cu_2O and CuO are shown at the top of the Figure.

It is worth noting that the Cu signals are seen higher in the pattern for the ED30 sample than in the other two films corroborating that thermal treatment results in a thick film composed of Cu_2O and CuO on which the CuO/Cu_2O core/shell nanorods are formed. Figure 2.8 contains a comparison of Raman spectra of hybrid CuO/Cu_2O nanorod arrays with that of the thermal precursor film, TH. The assignment of the characteristic Raman peaks for Cu_2O and CuO[102-104] are also indicated. Observe that the Raman peaks for the TH films are mainly dominated by the contribution of the CuO nanorod phase with only minor input from the dense Cu_2O under layer (Figure 2-8a). The progressive contribution of vibrations associated with the Cu_2O crystalline structure are clearly seen for TH/ED1 (Figure 2-8b) and TH/ED30 (Figure 2-8c) as the shell thickness increases with electrodeposition time. Concomitantly, the phonon peaks due to CuO practically disappear in the TH/ED30 film. Therefore, both XRD and Raman data corroborate that the CuO nanorods are progressively covered by Cu_2O crystallites in the hybrid samples (Figures 2-7 and 2-8).

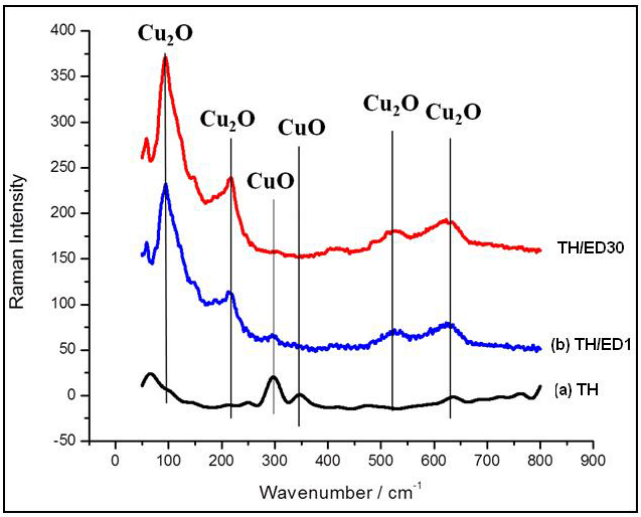

Figure 2-8 Comparison of Raman spectra of thermally oxidized film (a), a hybrid film with cathodic electrodeposition for 1 min (b), and a hybrid film with cathodic electrodeposition for 30 min (c). The nomenclature in the figure legend is that of Table 2.1.

2-3 Photoelectrochemical Performance of Hybrid CuO/Cu_2O Photocathode Samples

Figure 2-9 compares photocurrent/potential profiles for a TH/ED30 hybrid nanorod film (a) and an electrodeposited ED30 electrode (b) in CO_2-saturated 0.1 M Na_2SO_4 aqueous solution. The corresponding profile for an electrodeposited Cu_2O sample (ED30) in N_2-saturated solution under the same conditions is also included as control (c). The comparison of TH/ED30 (a) with ED30 (b) sheds important light on the role of the CuO interior core. Observe that throughout the potential range, the CuO/Cu_2O hybrid outperformed the electrodeposited ED30 control sample. Equally important is the fact that the photocurrent onset potential threshold was ~ 0.25 V more positive for the CuO/Cu_2O hybrid than the Cu_2O ED sample. The presence of the CuO (core) phase in the hybrid film clearly has contributed to this energetically favorable positive shift for the photoreduction reaction.

Another important trend in the data in Figure 2-9 is that the photocurrent/potential profiles of a Cu_2O electrodeposited film, (ED30, prepared on a polished Cu foil as substrate) showed a dramatic increase of photocurrent in the presence of CO_2 and also a positive shift of the photocurrent onset potential threshold. At -0.25 V vs. SHE, the photocurrent in CO_2-saturated solution was ca. 3.2 times higher than in the N_2 case. At less negative potentials the photocurrent enhancement in presence of CO_2 was much higher reaching factors of 6-7 at potentials ~ -0.1 V thus indicating that CO_2 is a much better electron scavenger (capturing the photoelectrons from Cu_2O) than water. The photoelectrochemical (PEC) performance of hybrid CuO/Cu_2O photocathodes prepared with different τ (10 and 30 min) at -0.1 V vs. SHE is compared in Figure 2-10 under manually chopped AM1.5 simulated solar illumination in CO_2- (a) and N_2-saturated (b) solutions.

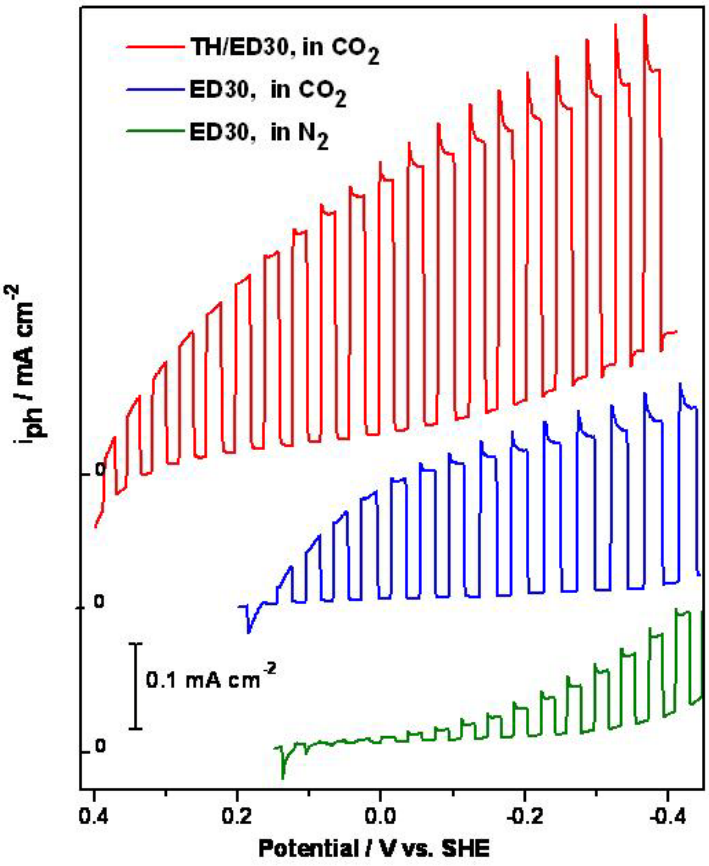

Figure 2-9 Comparison of PEC activity for TH/ED30 hybrid nanorod film (a) vs. an electrodeposited ED30 electrode (b) in CO_2-saturated 0.1 M Na_2SO_4 aqueous solution. The PEC activity for electrodeposited (ED30) in N_2-saturated solution (c) is also included for comparison.

In the N_2-saturated medium, the photocurrent is associated with H_2 photogeneration from water (blue traces in Figure 2-10). Importantly, in the CO_2 saturated electrolyte, the photocurrent transients for CuO/Cu_2O nanorod films are seen to reach ~3 times higher values than in the N_2-saturated counterpart solution (red traces in Figure 2-10a). Of all the hybrid CuO/Cu_2O samples, the TH/ED10 was found to perform

the best for the photoelectroreduction of CO_2 although the photocurrent transients have relatively higher spikes than in the TH/ED30 case.

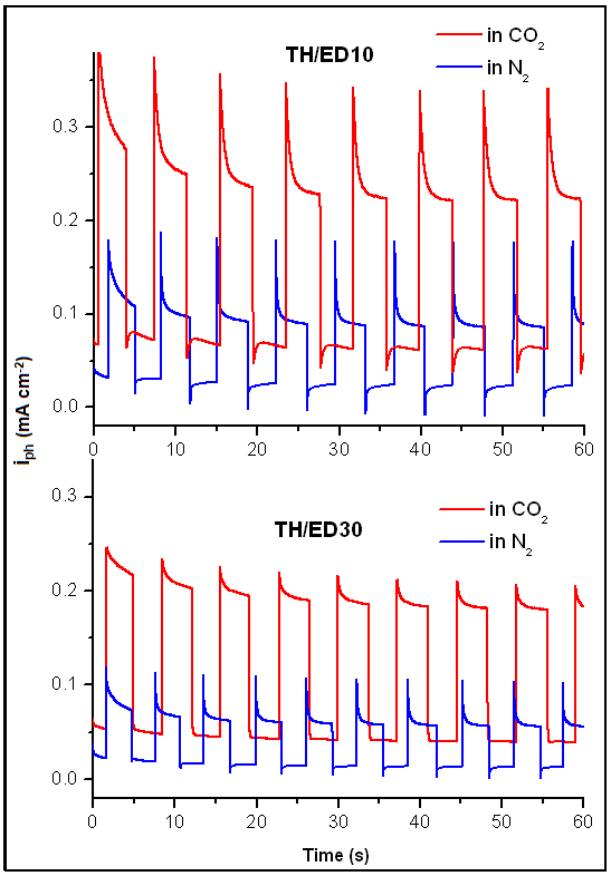

Figure 2-10 Photocurrent transients at -0.1 V (vs. SHE) of hybrid nanorod arrays under manually-chopped simulated AM1.5 illumination (70 mW cm^{-2}) for TH/ED10 and TH/ED30 electrodes in CO_2- (a) and N_2-saturated (b) aqueous solution containing 0.1 M Na_2SO_4 as electrolyte.

Figure 2-11a presents a bar diagram comparison of the photoactivity as manifested by transient, stationary and net photocurrents for CuO/Cu_2O photocathodes in CO_2-saturated aqueous solution. The hierarchical CuO/Cu_2O core/shell nanorod arrays

all show enhanced photocurrent in CO_2 saturated solutions with respect to the TH film, pointing to efficient removal of photogenerated electrons from Cu_2O to the CuO core.

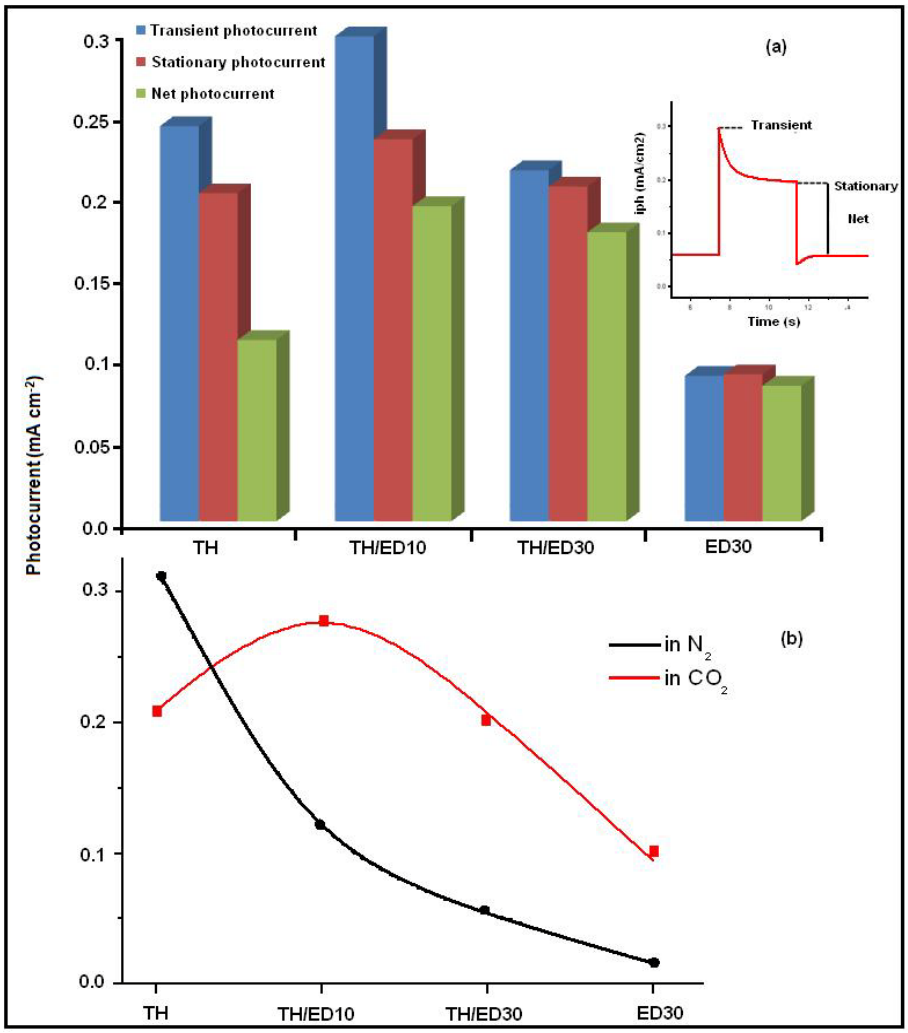

Figure 2-11 (a): Comparative bar diagram of transient, stationary and net photocurrent for TH, TH/ED10, TH/ED30 and ED30 photocathodes in CO_2-saturated 0.1 M Na_2SO_4 as electrolyte. Applied potential = -0.1 V vs. SHE. Illumination = AM1.5 solar simulator. The inset clarifies the nomenclature for transient, stationary and net photocurrent. (b) Comparative plot of stationary photocurrent for TH, TH/ED10, TH/ED30 and ED30 under N_2 and CO_2 respectively.

Figure 2-11b compares stationary photocurrent at -0.1 V for CO_2 and H^+ photoelectrochemical reduction: the TH films yielded higher photocurrent than any of the TH/EDτ (τ varied between 1 and 30 min) hybrid counterparts for H_2 evolution, but the TH films progressively deteriorated in their PEC performance as the CuO nanorods became covered by electrodeposited Cu_2O.

2-4 Performance and Stability of Nanorods during the Photoelectrosynthesis of Methanol

Photoelectrosynthesis of CH_3OH was demonstrated with a TH/ED10 CuO/Cu_2O nanorod photoelectrode. The photoelectrode was placed in 100 mL electrolyte solution saturated with CO_2, polarized at -0.2 V vs. SHE, and continually irradiated with visible light provided by a AM1.5 solar simulator. The irradiated electrode area was ca. 3 cm^2. Representative photocurrent/time and charge/time profiles recorded during the photoelectrolysis are shown in Figure 2-12a and b respectively.

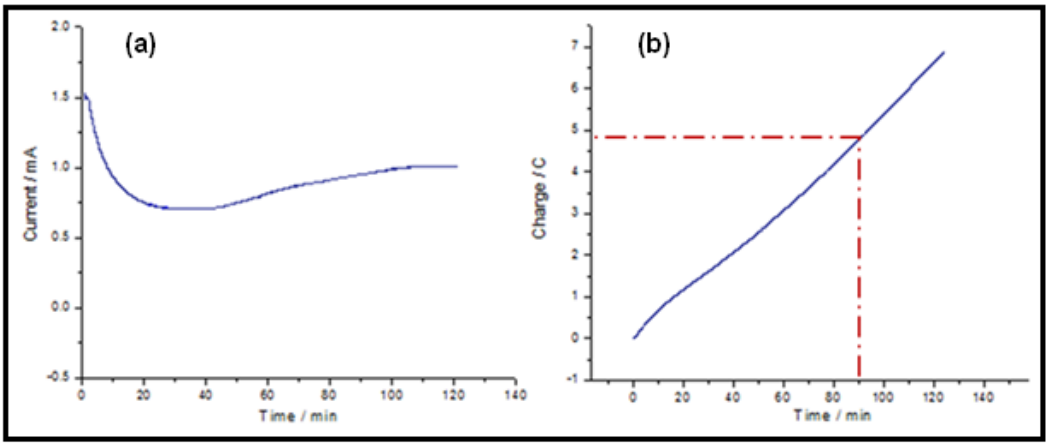

Figure 2-12 Current/time (a) and charge/time (b) profiles under continuous solar irradiation at -0.2 V vs. SHE in a sealed two-compartment photoelectrochemical cell containing a TH/ED10 nanorod photocathode. Electrolyte was 0.1 M $NaHCO_3$ saturated with CO_2 and maintained at room temperature.

Observe in Figure 2-12 that the photocurrent decreases during the first 30 min and then recovers to reach a constant value of 1.05 mA at ~ 2 h of irradiation. Even if some photocorrosion had occurred leading to formation of metallic copper on the electrode surface, this process did not diminish the performance of the CuO/Cu_2O photoelectrodes. Note, that dark current values at least an order of magnitude lower (0.10 mA) than the photocurrent level corroborate that the electrode remained photoactive throughout the photoelectrolysis duration.

To analyze the photoelectrogenerated product, liquid samples were periodically withdrawn from the photoelectrochemical cell. A gas chromatograph equipped with a mass spectrometer (GC-MS) was used to detect methanol. Chromatographic results of four different photoelectrosynthesis samples together with a calibration curve, performed with several known methanol concentrations, are presented in Figure 2-13. By comparing the highest intensity obtained from the MS spectra (Figure 2-13a) which is about 35000 with the calibration curve equation (Figure 2-13b) the maximum amount of methanol was calculated. Methanol photogeneration was monitored at m/z = 31 amu (CH_2OH^+) and was found to reach a concentration of ca. 85 μM after 90 min of continuous solar irradiation (from a solar simulator). Faradaic efficiencies were in the 94-96 % range (considering that 6 e^- are required to form one molecule of CH_3OH from CO_2). Note that a potential of -0.2 V vs. SHE represents an "underpotential" greater than at least 150 mV given that the standard potential for the CO_2/CH_3OH redox process lies at -0.38 V vs. SHE at pH 7. The main reason to chose m/z = 31 for the detection of methanol in the study was the highest intensity associated with this fragment versus the other fragments shown in the standard methanol MS spectrum.[105]

For further confirmation of methanol production GC-MS head space (at 75°C) was carried out. In this process after the liquid aliquot was taken for the supporting

electrolyte removal the remaining solution which was sealed completely in a flask, was heated in a water bath to the boiling point of methanol (at ~ 75-80 ^{0}C) and the respective gas samples were then transferred to vacuumed vials for analysis in GC-MS using an injection volume of 5 µl. Figure 2-14 illustrates the methanol peak in1.53 min for m/z=31.

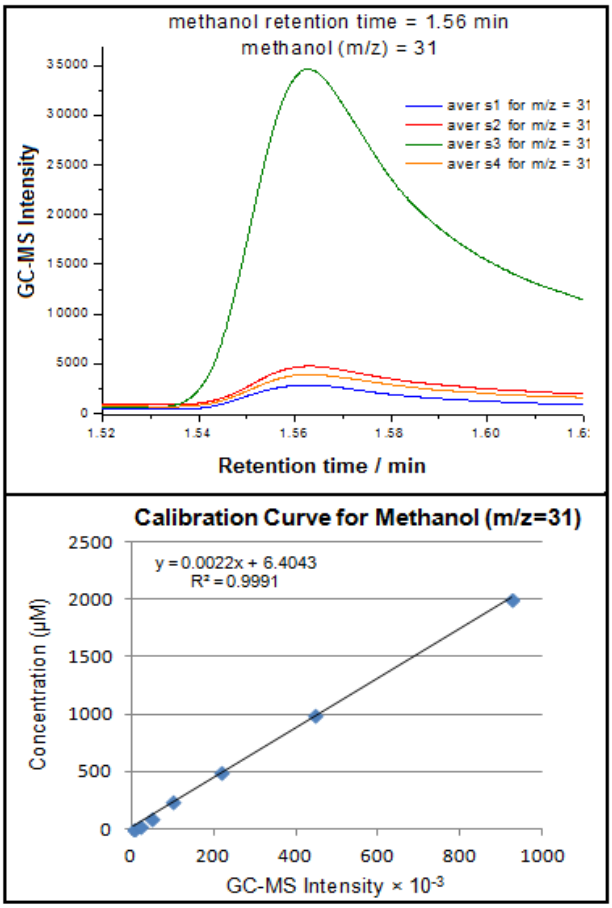

Figure 2-13 Chromatographic results for 4 different photoelectrosynthesis processes after 90 min irradiation (a) calibration curve of methanol samples with the concentration range from 5µ M to 2 mM in water (b).

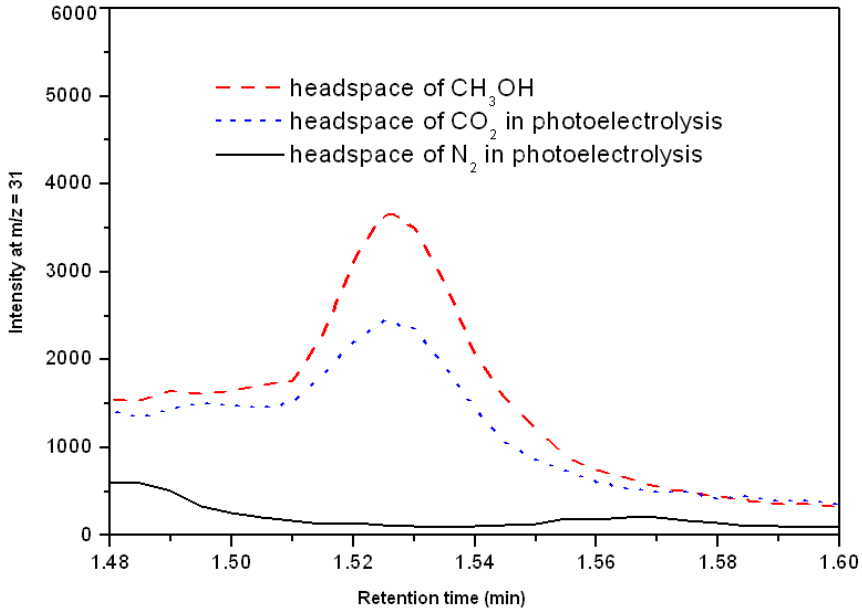

Figure 2-14 Head space spectra of a sample with known concentration of methanol (red trace) in comparison with the photoelectrosynthesis samples under N_2 (black trace) and CO_2 (blue trace) bubbling.

To link stability with photoactivity of the hybrid nanorod photoelectrode during photoelectrogeneration of methanol from CO_2, XRD patterns were obtained as a function of photoelectrolysis time and compared with the pattern for the pristine photoelectrode before irradiation (Figure 2-15). Observe that before photoelectrolysis (Figure 2-15a), three distinguished crystalline structure are clearly discernible: CuO, Cu_2O and Cu. As the hybrid photoelectrode was prepared from a copper foil, the Cu metal diffractions, associated with the underlying substrate are also seen in the pattern.

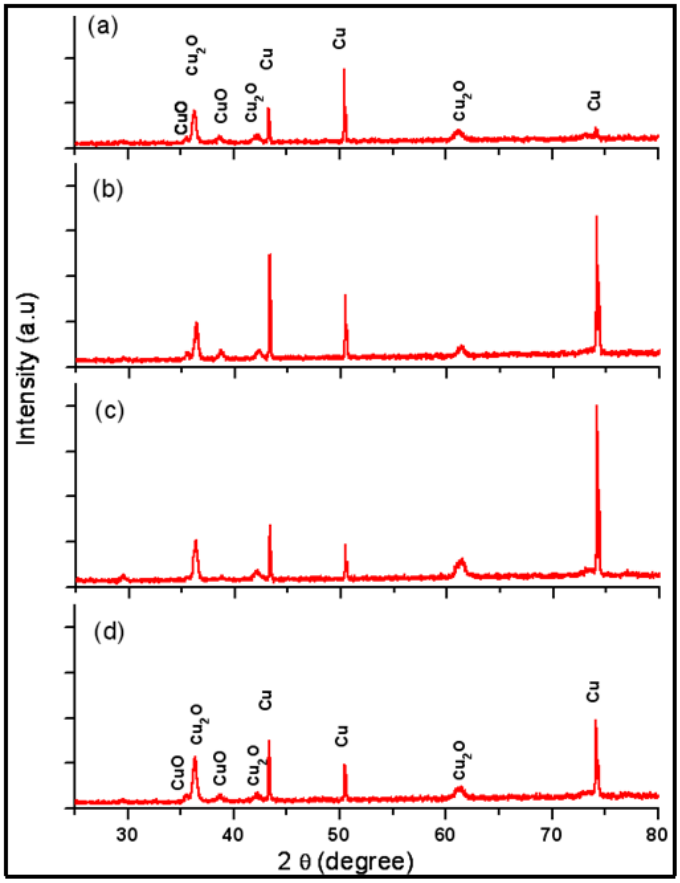

Figure 2-15 XRD spectra of a TH/ED10 CuO/Cu_2O hybrid nanorod film before (a) and after being subjected to photoelectrolysis at -0.2 V vs. SHE in a CO_2-saturated aqueous solution for 30 (b), 60 (c) and 120 min (d). The Cu/Cu_2O nanorod film was prepared on a copper foil whose XRD peaks are clearly discernible before and after photoelectrolysis.

Because of the photoelectrolysis, the Cu peak at $2\theta = 74.1°$ associated to a (220) orientation is the one seen more affected and it grows progressively at 30 and 60 min and then recede at prolonged electrolysis (120 min). This peak seems therefore to be detecting the formation of surface Cu^0 by photocorrosion of the respective Cu_2O (220) face seen at $2\theta = 61.3°$.

When the photoelectrolysis duration reaches 30 min (Figure 2-15b) the Cu_2O and CuO peaks remain unchanged while the Cu^0 diffraction peaks at 43.2° and 74.1° are higher. It points to incipient formation of metallic Cu from self-reduction of the photoelectrode surface. However, as photoelectrolysis continues, the Cu peak located at 74.1° shows the largest variation at times of 60 min (Figure 2-15c) and 120 min (Figure 2-15d) of photoelectrolysis respectively.

This peak shows a temporal evolution quite similar to the photocurrent evolution in Figure 2-12a. At shorter times (up to 60 min), the photoelectrode is covered by Cu (due to photocorrosion) but then a "self-healing" process counters metal accumulation; i.e., the metal phase undergoes chemical corrosion to regenerate the oxide phases. The photocurrent-time profile over a 2 h time frame (Figure 2-12a) is also diagnostic of possible slow self-healing of the photocathode assembly as the oxide phases are regenerated when the photoelectrons exit the interfacial phase boundary to CO_2. In fact, the photogenerated electrons presumably are rapidly transferred to CO_2 before they have an opportunity to *appreciably* photoreduce Cu(I) or Cu(II) in the oxides to the metallic state.

There might be a possibility in which the methanol could originate from decomposition of the lactic acid that may have leached out of the Cu_2O film during the PEC experiments. This argument rests on the presumed entrapment of lactate species in the oxide film during its electrodeposition history. However careful analyses of electrochemically grown Cu_2O films using quartz crystal microgravimetry data[106] are unambiguous in the lack of trapped lactate species in the film. Previous authors[69,107,108] have also used surface analyses and other means to conclude the lack of lactate (or other electrolyte species such as sulfate, chloride, or phosphate) entrapment in the electrodeposited Cu_2O films.

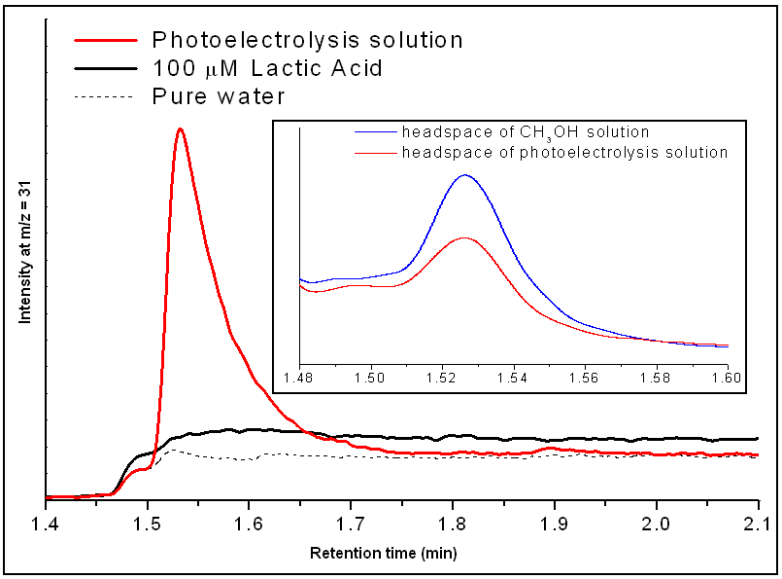

Figure 2-16 Chromatographic result of photoelectrolysis solution (red trace), 100 M lactic acid in water (black trace) and, pure water (dotted trace) to confirm the methanol production from the CO_2 reduction not lactic acid entrapment. The inset box demonstrates the head space results for the sample of known concentration of methanol (blue trace) and the photoelectrosynthesis sample (red trace).

To confirm that the methanol peak observed in our GC-MS experiments above originated from CO_2 and not from other adventitious sources such as lactate the following control experiments is were carried out. Aliquots were withdrawn after 90 min PEC runs in (a) blank in the absence of CO_2 in 0.1 M Na_2SO_4, dotted trace, (b) 100 μM lactic acid, black trace, and (c) photoelectrolysis solution, red trace, and worked up for GC-MS analyses as is illustrated in Figure 2-16. Presence of the 1.53 min methanol peak (at m/z = 31) was unmistakable in the GC-MS data for (c) but was absent in the other two (a and b) cases. Another set of experiments this time using head-space sampling at 75-80 °C showed clear evidence that the methanol must have originated from the photoreduction

of dissolved CO_2 and not from the decomposition of any adventitious organic species in the electrolyte (inset of Figure 2-16). It is worth noting that methanol has high vapor pressure under these conditions while that of lactic acid (boiling point: ~ 200 °C) is virtually negligible.

Thus even in the unlikely scenario (see above) that lactate species leach out from the oxide film during PEC reduction runs, the above data furnish evidence for the fact that they cannot generate methanol either thermally or from the PEC oxidation of lactate (to CO_2). Unlike TiO_2 for example, the valence band in Cu_2O is situated too "high" to sustain significant PEC oxidation of the lactate species.

2-5 Interphasial Charge Transfer in CuO/Cu_2O

The photoreduction of CO_2 to methanol is assisted by the favorable band-edge alignment of both oxide phases as depicted in the diagram in Figure 2-17. Note that the valence band of CuO is located positive of the corresponding level in Cu_2O in full agreement with the photocurrent/potential response of a CuO/Cu_2O hybrid nanorod electrode and that of a single Cu_2O film (Figure 2-9). Therefore, in a Cu_2O/CuO core/shell nanorod configuration, the differences in the band edges of the two oxides translate to a vectorial transfer of photogenerated electrons from the Cu_2O shell to the CuO core. As the Cu_2O shell is also in contact with the electrolyte, the photogenerated electrons in Cu_2O are able to be directly transferred to CO_2 as indicated in Figure 2-17. This double pathway for injection of photoelectrons to CO_2 is likely a contributor to the enhanced photoelectrochemical performance of CuO/Cu_2O nanorod arrays relative to a single phase Cu_2O film. Additionally, the increased surface area of the CuO/Cu_2O with respect to a compact Cu_2O ED film is certainly an additional factor in the photocurrent enhancement. Importantly to sustain the double injection pathway the tip of the CuO core has to be in contact with the electrolyte.

The relevant potentials for photocorrosion of Cu_2O and CuO are also shown in the same diagram. These data were taken from literature sources[109-112] after suitable correction for the reference electrode potential scale. Note that both photocathodic corrosion of Cu_2O (generating metallic Cu as the product) and photoanodic oxidation of Cu_2O to CuO have been discussed in the literature.

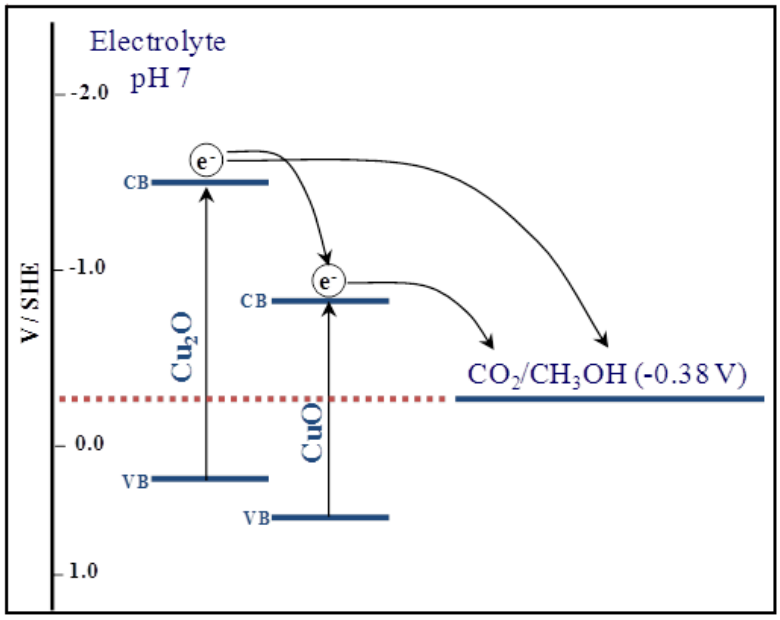

Figure 2-17 Energy band diagrams of hybrid CuO/Cu_2O nanorod arrays for solar photoelectrosynthesis of CH_3OH from CO_2. Semiconductor band edges and redox potentials are shown vs. SHE. CB, conduction band; VB, valence band. The oxide photocorrosion potentials were obtained from data in Refs. 110-114.

2-6 Conclusion

A simple two-step hybrid thermal growth/electrodeposition approach was employed to prepare and optimize solar photoactive CuO/Cu_2O nanorod arrays for the photo-electrosynthesis of methanol from CO_2. These hybrid photocathodes were shown to possess a suitable geometry and chemical composition consisting of a Cu_2O shell

covering the support CuO nanorod and with appropriate length and high aspect ratio for optimal transport and collection of photogenerated electrons. Methanol photogeneration was confirmed by GC-MS analyses of product evolved at -0.2 V vs. SHE, i.e. at an *underpotential* relative to the standard potential of CO_2/CH_3OH. This last feature is an important virtue of the p-type semiconductor based photoreduction approach as adopted in this study and by other authors[61-63] previously. In contrast the ("dark") electrocatalytic process counterpart for CO_2 reduction suffers from the electrical energy cost incurred from the need for considerable *overpotentials* to overcome the kinetic barrier associated with this process.[113,114]

Chapter 3

Electrochemical Study of 1, 3 - Diamine Flavin

Flavins are unique compounds in nature which take part in many biochemical reactions as coenzymes and photoreceptors.[72] The redox properties of flavins have been studied since 1900 and it is well known that the fully oxidized flavoquinone is immediately reduced to flavohydroquinone in a two-electron and two-proton process.[73,91] The electrochemical behavior of flavins on modified electrode surfaces including, platinum (Pt)[75], gold (Au)[87,115-118], glassy carbon[77,78,88,90,119,120], mercury (Hg)[85,121] and titanium dioxide (TiO_2)[86,122-125] has been extensively investigated.

Herein the electrochemical properties of newly synthesized Flavin, - bis (2,2,2-trimethylammoniumethyl) - alloxazine dibromide, (thereafter denoted as Fl^{2+}) was studied on three different types of electrode materials including, glassy carbon (GC), gold (G) and copper / copper oxide (Cu/Cu_2O). Cyclic voltammetry (CV) was used to determine the interaction of Fl^{2+} with the electrodes in terms of redox potentials and reduction reaction control (surface vs. mass transport).[3] The speciation and mechanistic details of the electroreduction and protonation of Fl^{2+} in aqueous electrolytes was studied at selected pHs in the range from 1 to 10. Spectroelectrochemistry was performed in integral and differential modes to determine the mechanistic details of this electroreduction process. The electrochemical reactions were carried out under dark and light conditions to observe whether or not light has any effect on the redox behavior of this compound. Also, the electrocatalytic performance of Fl^{2+} when the electrolyte was saturated with different gases such as, oxygen (O_2) or carbon dioxide (CO_2) was obtained and compared with blank runs under same electrolyte conditions but saturated with nitrogen (N_2).

3-1 Experimental

3-1-1 Synthesis

Flavin was synthesized by the modification of literature procedures.[126,127] The tricyclic core of Fl^{2+} was prepared by the condensation of commercially available phenylene diamine and alloxan monohydrate (Figure 3-1a and b respectively). Subsequent preparation of the alloxazine dipotassium salt (Figure 3-1d) allowed for the careful alkylation at the 1 and 3 positions. All other conventional methods of 1,3-alkylation led to N-dealkylation of dimerization of the ammonium reagent. The compound (Figure 3-1e) was purified by filtration followed by washing with suitable solvents until spectroscopically pure by TLC and NMR. A scheme for the synthesis of the Fl^{2+} is shown in Figure 3-1a-e.[127]

All chemicals and reagents used in the synthesis as well as in electrochemical runs were of analytical grade, and used as received without further purification. The supporting electrolyte, used for electrochemical experiments, was 0.1 M sodium sulfate (Na_2SO_4) and prepared by using doubly distilled deionized water. Prior to each experiment, the solutions were saturated by purging with different gases depending on the purpose of the experiment.

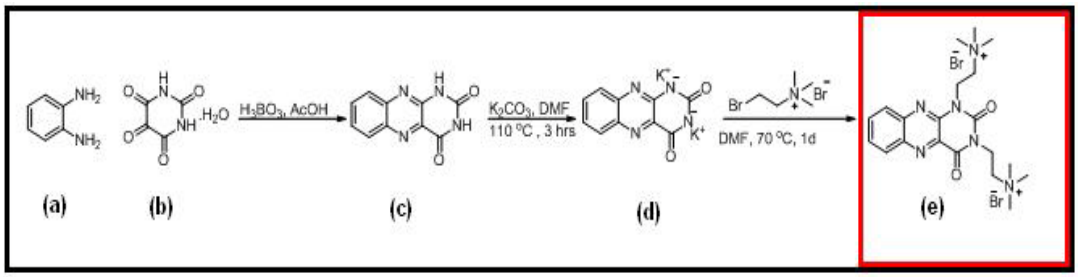

Figure 3-1 Schematic illustration of the synthesis for 1,3-diamine flavin (Courtesy of Mohammad Shawkat Hoessain).

3-1-2 Electrochemistry and Spectroelectrochemistry

Electrochemical measurements were performed with CH Instruments Model-600C using a conventional three-electrode electrochemical cell. Three different electrode materials (GCE, G, and Cu/Cu_2O) were used as working electrode in the process. The GCE and G (2.0 mm diameter disk in both cases) from Bioanalytical Systems and a Cu/Cu_2O film, where Cu_2O electrodeposited on copper foil, (thickness of 1.0 mm and area of 2.0 mm^2, see Chapter 2), from Basic copper were used. Immediately before use, both GC and G electrodes were polished to a mirror finish with wet alumina (Buehler, 0.05 μm), followed by rinsing with doubly distilled deionized water. The copper electrode either when used alone or before electrodeposition was cleaned using 1 M HCl, acetone, isopropanol and then it was sonicated in doubly distilled deionized water. A platinum wire was used as counter electrode. All the electrode potentials were measured with respect to an Ag/AgCl [KCl (sat.)] reference electrode.

The ultraviolet-visible (UV-Vis) absorption spectra were obtained by using a diode-array spectrophotometer (Hewlett-Packard model 8453). Transmittance UV-Vis spectroelectrochemical measurements were performed in a quartz thin-layer cell containing a gold minigrid as working electrode. The Fl^{2+} solution with a concentration of 2.5 mM located in the thin-layer space was spectroscopically probed by using the diode-array spectrometer during slow cyclic potential scans (5 mV/s) encompassing the Fl^{2+} electroreduction potential window. The counter electrode (platinum wire) and a miniature Ag/AgCl [KCl (sat.)] reference electrode were laterally placed in the quartz cuvette next to the thin-layer compartment. The top part of the cell consists of Teflon stopper with tight perforations for electrodes as well as connectors for degassing.

3-2 Copper / Copper Oxide Electrodes

3-2-1 Voltammetric Behavior of Fl^{2+} with Cu and Cu/Cu_2O Electrodes

To study the electrochemical behavior of Fl^{2+} on copper-based electrodes, a metallic copper foil was immersed in the electrochemical cell containing a solution of 0.1 M sodium sulfate (Na_2SO_4) at pH 7.0 and purged with N_2 for about 10 minutes. CV experiments were performed on the blank solution (only electrolyte) from the initial potential of -0.1 V to final potential of -0.6 V vs. Ag/AgCl reference electrode. Then a specific amount of Fl^{2+} was added to the electrolyte to make 0.1 mM concentration and the solution was thoroughly purged first with N_2 and then O_2; after which the respective CV experiments were performed on both solutions. Resulting voltammograms are shown in Figure 3-2. By comparing the two voltammograms related to the solutions with and without the compound under N_2 saturation, it is obvious that the presence of the Fl^{2+} does not affect the voltammogram when using a metallic copper electrode. However, in the voltammograms containing 0.1 mM Fl^{2+} under N_2 and O_2 saturation a large increase in the current have shown for the O_2 saturated solution.

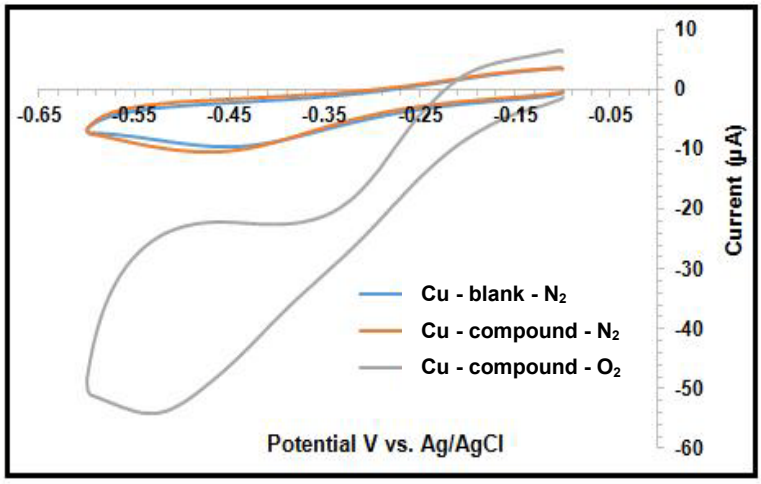

Figure 3-2 Cyclic voltammogram of Cu electrode in 0.1 M Na_2SO_4 containing 0.1 mM Fl^{2+} under O_2 and N_2 saturation and the blank voltammogram under N_2 saturation, for the scan rate of 0.02 V/s.

The reason for that increase is mainly associated to the electroreduction of copper oxide formed on the Cu surface in contact with oxygen and not highly affected by the presence of the Fl^{2+} in the solution.

The CV experiment with the copper electrode did not provide observable effects upon addition of Fl^{2+} to study the behavior of this compound so the next step was to make a copper oxide film on the copper substrate to investigate if any changes will happen by using a copper oxide film as a photoelectrode. Copper oxide films were prepared using the electroreduction method that was described in Chapter 2.[97]

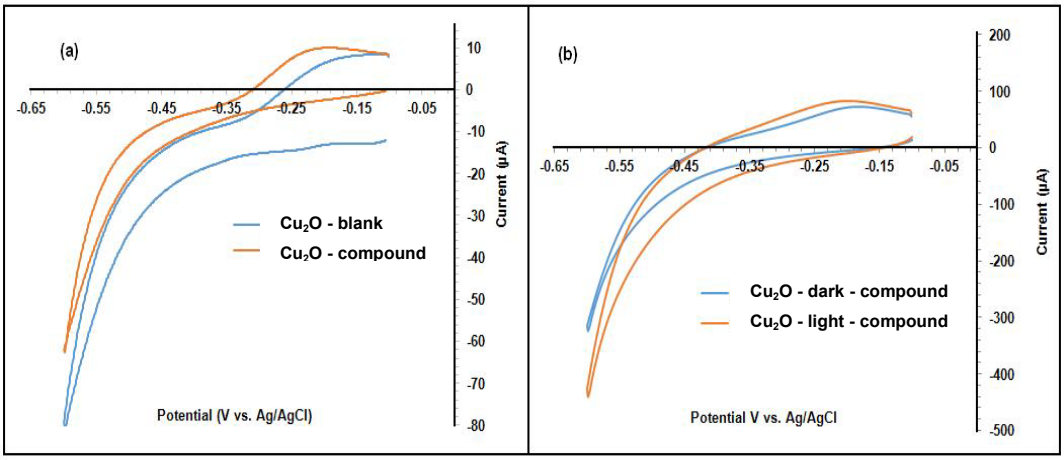

Figure 3-3 Cyclic voltammogram of Cu_2O electrode with and without Fl^{2+} (a), cyclic voltammogram of Cu_2O electrode in a solution containing 0.1 mM Fl^{2+} under dark and solar radiation conditions (b), both under N_2 bubbling.

Voltammograms of the CV experiment with copper oxide (Cu_2O) electrode are shown in Figure 3-3. A comparison between the CV of a solution with and without Fl^{2+} on the Cu_2O electrode in Figure 3-3a shows that there is no effect of the organic compound while using the Cu_2O electrode. Although copper oxide films are known as oxide semiconductors, Figure 3-3b reveals that there were no significant changes in the current

magnitude between the profiles obtained under light conditions compared to the dark reaction conditions.

In conclusion, the metallic copper (Cu) and the copper oxide (Cu_2O) electrodes were not considered for further investigation of the electroreduction behavior of Fl^{2+} because the compound does not show significant electroactivity on these electrode substrates neither under dark nor light irradiation. We speculate that the Cu electrode is itself covered by a native Cu_2O film and therefore it behaves as a semiconductor electrode like in the case when the electrodeposition of Cu_2O was performed. Therefore in both cases, no response to a redox electroactive species in solution under dark is expected (see Figure 3-3a where the presence of Fl^{2+} brings in fact a cathodic current decrease and likely pointing out to a surface blockage of the electrode by the Fl^{2+} species which inhibit the organic compound electroreduction). Under the irradiation of visible light, the cathodic current is slightly higher than in dark (Figure 3-3b) and likely associated to a combination of water as well as Fl^{2+} photoelectroreduction. Another fact that this study cannot utilize Cu/Cu_2O electrodes is simply because the potential for Fl^{2+} redox process, as it will be discussed later (-0.63 V vs. Ag/AgCl), is more negative than the potential window where the copper oxide is stable (i.e. cannot go more negative than -0.6 V vs. Ag/AgCl).

3-3 Gold Electrode

3-3-1 Voltammetric Behavior of Fl^{2+} on Gold Polycrystalline Electrode

A Gold electrode (2.0 mm diameter) was considered as the second alternative material for the study of the Fl^{2+} compound. Initial experiments were consisted of utilizing a gold electrode to perform CVs on the supporting electrolyte (blank solution) and then the electrolyte containing 0.1 mM of the compound. The voltammogram containing 0.1 mM Fl^{2+} shows a redox couple at -0.63 V vs. Ag/AgCl for the scan rate of 0.02 V/s

(shown in Figure 3-4). The voltammetric shape of this process points out to a diffusion-controlled reaction[3] containing the corresponding cathodic and anodic redox peaks on gold electrodes and it was encouraging us to lead a more thorough investigation of the electrochemical behavior of this organic molecule.

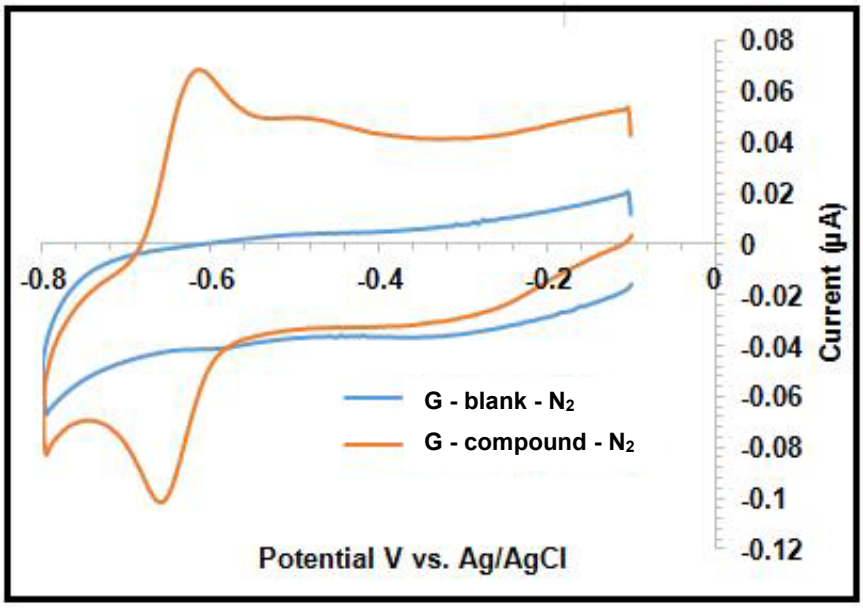

Figure 3-4 Cyclic voltammogram of gold electrode in 0.1 M Na_2SO_4 (blue trace) and in the electrolyte containing 0.1 mM Fl^{2+} (red trace) under N_2 saturation.

Cyclic voltammetry was performed in the potential range between -0.1 and -0.8 V vs. Ag/AgCl reference electrode for different scan rates from 0.01 V/s to 0.08 V/s in a 0.1 M Na_2SO_4 solution containing 0.1 mM Fl^{2+}, as represented in Figure 3-5a. The results illustrate that the Fl^{2+} compound is electrochemically reversible in aqueous solutions when using a bare gold electrode. The Fl^{2+} reduction is confirmed to be a diffusion-controlled process, because of the linear dependence of the cathodic and anodic peak currents to the square root of scan rate (Figure 3-5b).

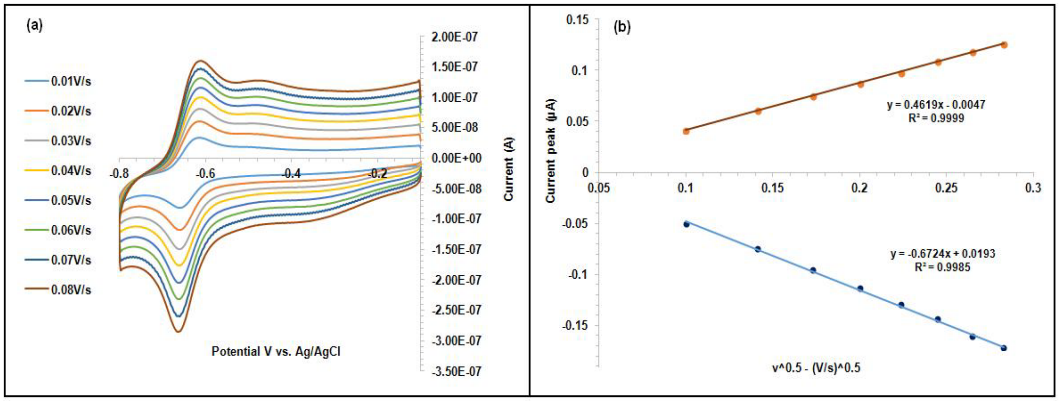

Figure 3-5 Cyclic voltammogram of gold electrode in a solution containing 0.1 mM Fl^{2+} for different scan rates under N_2 bubbling (a) cathodic and anodic peak currents versus square root of scan rate (b).

The ratio of cathodic/anodic peak currents at various scan rates is almost constant (i_{pc}/i_{pa} ~ 1.0) which indicates a reversible redox reaction. The peak to peak potential separation, ΔE_p at 25 °C, is about 58 mV versus scan rate (V/s), suggests a facile charge transfer in the process.[3]

3-3-2 Effect of pH on the Voltammetric Behavior of Fl^{2+}

The effect of pH on the gold electrode was investigated by recording cyclic voltammograms using 0.1 M Na_2SO_4 at various pH values from 2 to 10. Figure 3.6 shows the comparison of cyclic voltammograms recorded at different pH values for the scan rate of 0.02 V/s and the electrolyte was purged with N_2 before each scan to make sure that there will not be oxygen interference in the reaction.

These voltammograms show that the Fl^{2+} compound exhibits a single redox couple in aqueous media at the pH range from 2 to 10. With an increase in the pH, the compound's reduction and oxidation peaks are shifted towards negative potentials, indicating that the compound redox reaction is proton concentration dependent.

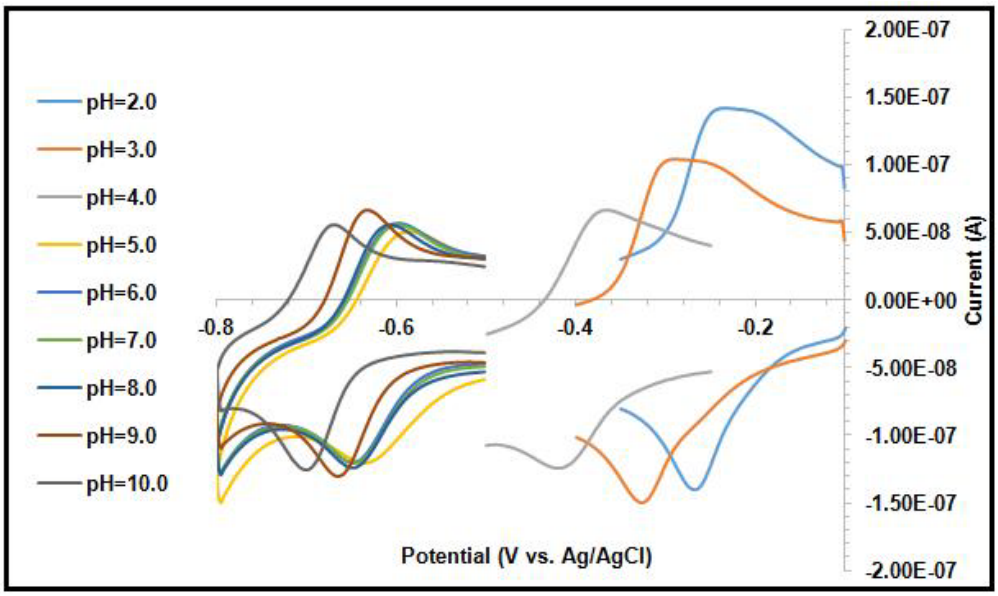

Figure 3-6 Effect of pH on the cyclic voltammograms of Fl^{2+} at gold electrode in an aqueous solution of 0.1 M Na_2SO_4 adjusted to selected pHs in the range from 2 to 10 for the scan rate of 0.02 V/s.

The dependency of formal potential of the redox reaction, $E^{o'}$, on the pH of supporting electrolyte for the compound is plotted versus pH in Figure 3-7. At acidic pH (< 4) the slope of the $E^{o'}$ vs. pH is 71 mV per pH unit which indicates a two electron -two proton process (see the respective equations inserted in Figure 3-7).[3] At pH more basic than pH 7, the slope of formal potential vs. pH is 29 mV per pH unit which corresponds to an electrode process involving two electrons and one proton. At pHs in the range of 5 to 7, $E^{o'}$ was found to be mainly constant.

This behavior suggests that the electroreduction reaction always involves two electrons but the number of protons is directly dependent on the pH of the electrolyte. When protons are abundantly available in the solution (acidic solutions) the reaction goes

to a completion of two electrons and two protons process. If fewer protons are available in the reaction two electrons are transferred with only one proton.

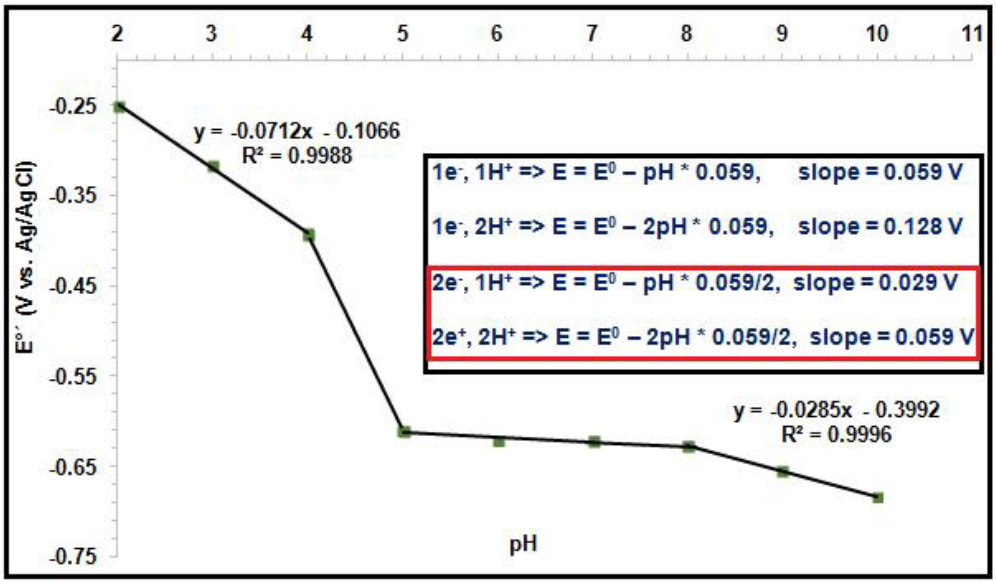

Figure 3-7 dependence of Fl^{2+} formal potential with respect to pH of the supporting electrolyte and in the pH range from 2 to 10.

3-3-3 Electrocatalytic Reduction of Oxygen

So far, the gold electrode has demonstrated promising results for the study of this organic compound (Fl^{2+}). When it comes to oxygen reduction reaction (ORR) on a bare gold electrode, no significant electrocatalytic activity is displayed from the organic compound because the gold electrode itself competes against the compound for the ORR. Figure 3-8 presents a cyclic voltammogram of gold electrode in a solution containing 0.1 M Na_2SO_4 saturated with O_2 with and without the 0.1 mM Fl^{2+}. The broad peak at about -0.55 V vs. Ag/AgCl corresponds to the ORR directly on gold and the presence of the organic compound increases the current in only ~ 20% thus it indicates that the main ORR occurs on the gold electrode and not by the intermediate effect of the

Fl^{2+} compound. One of the most common ways to eliminate the interaction of the gold electrode with the O_2 is to modify the surface of the electrode. Gilbert Noll has investigated the behavior of flavoproteins with flavin-modified gold electrodes.[117,118]

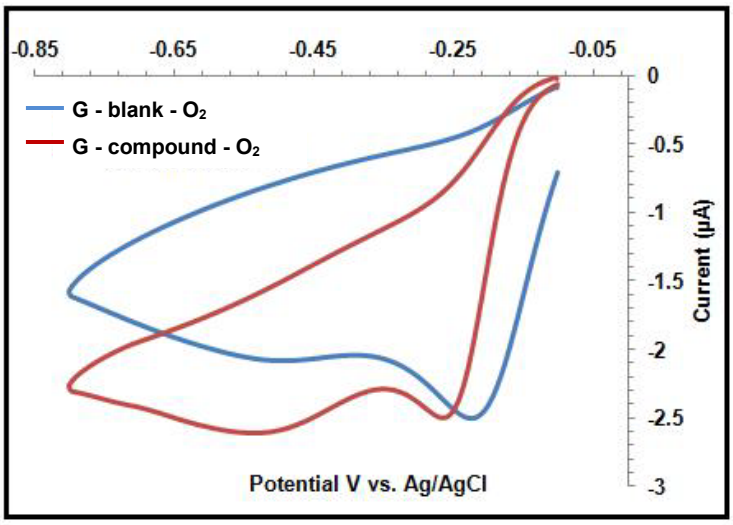

Figure 3-8 Cyclic voltammograms of gold electrode in a 0.1 M Na_2SO_4 saturated with O_2 with and without the compound for 0.02 V/s scan rate.

3-4 Glassy Carbon Electrode (GCE)

After eliminating copper/copper oxide and bare gold electrodes for the thorough study of this Fl^{2+} compound, glassy carbon turned out to be the best material for this study. First, the potential window that it can be used is wider than in copper oxide films and second, oxygen (O_2) will not interact with the electrode surface as it is the case in gold electrode therefore, it will demonstrate the activity of Fl^{2+} on ORR. CV was first conducted on the GCE in 0.1 M Na_2SO_4 in the presence and absence of Fl^{2+} in a potential range from -0.1 to -0.8 V vs. Ag/AgCl as represented in Figure 3-9. The voltammogram containing Fl^{2+} shows a redox couple at -0.63 V vs. Ag/AgCl for the scan rate of 0.02 V/s. It is worth noting that the blank voltammogram shows a larger double layer capacitance than in the presence of the Fl^{2+} compound.

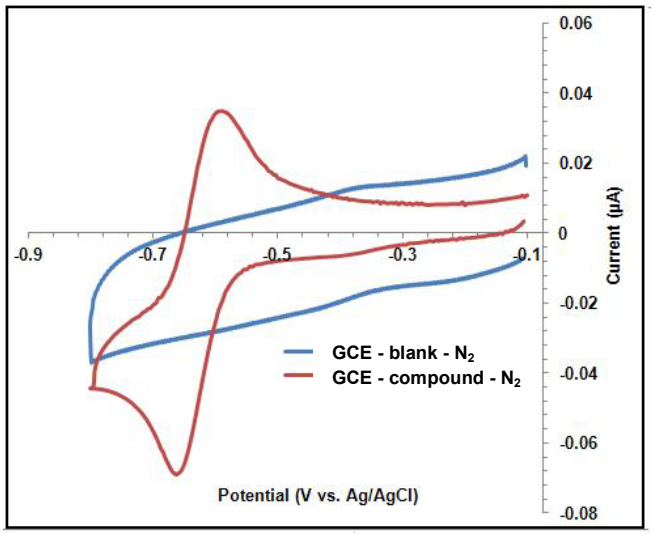

Figure 3-9 Cyclic voltammogram of glassy carbon electrode in the electrolyte (blue trace) and in the electrolyte containing 0.1 mM Fl^{2+} (red trace) under N_2 saturation for the scan rate of 0.02 V/s.

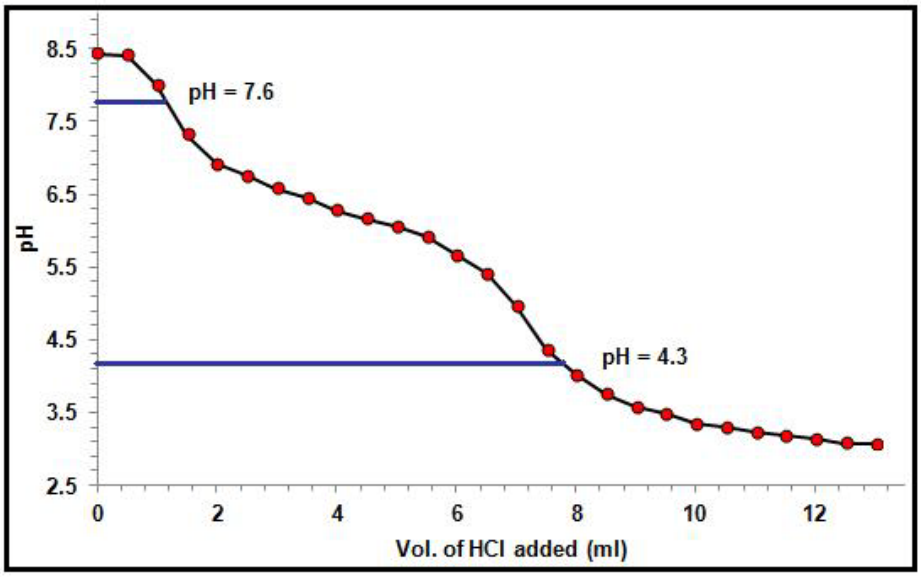

Figure 3-10 titration curve was obtained by addition of 13.00 ml of HCl to the solution containing 0.01 M Fl^{2+} compound.

In order to select different pHs for investigation the behavior of Fl^{2+}, a titration curve was obtained. This curve was obtained by successive aliquot addition of 0.001 M hydrochloric acid (HCl) to the solution containing 0.01 M Fl^{2+}. Initial pH was 8.50 and after addition of 13.00 ml HCl the final pH reached to 3.00 as it is represented in Figure 3-9. Three regions were observed in the titration curve, showing two protonation steps and therefore three different pHs (pH = 3, 7, 9) were chosen to study the behavior of Fl^{2+}. Because of the similarities between pH 7.0 and 9.0 the graphs for pH 7.0 are not shown in Figure 3-11.

3-4-1- Voltammetric Response of Fl^{2+} with Glassy Carbon Electrodes

The redox behavior of Fl^{2+} using a GCE was investigated by performing cyclic voltammetry on solutions with three targeted pHs (3.0, 7.0 and 9.0). Figure 3-11 shows representative cyclic voltammograms of Fl^{2+} (0.1 mM) recorded in 0.1 M Na_2SO_4 with increasing scan rates encompassing a potential range between -0.8 and 0.1 V for pH 3.0 and -0.8 and -0.1 V for pH 7.0 and 9.0 respectively. The potential window for acidic pH is smaller than that of basic pH. The reason for that is the high concentration of protons in the solutions which leads to hydrogen evolution in the system. As it is shown in Figure 3-11, at all pHs (pH 7.0 is not shown) a reversible redox couple is obtained. Similar voltammograms were also run in an ample pH range from pH 1 to pH 10 and for all of them the potential range was chosen to completely cover the electroreduction of Fl^{2+}. At all three pHs, the voltammetric curves illustrate that the Fl^{2+} electrode process is electrochemically reversible on glassy carbon electrode although the electrode process seems more complex at acidic pHs as shown by the splitting of the oxidation peak during the returning scan at pH 3.

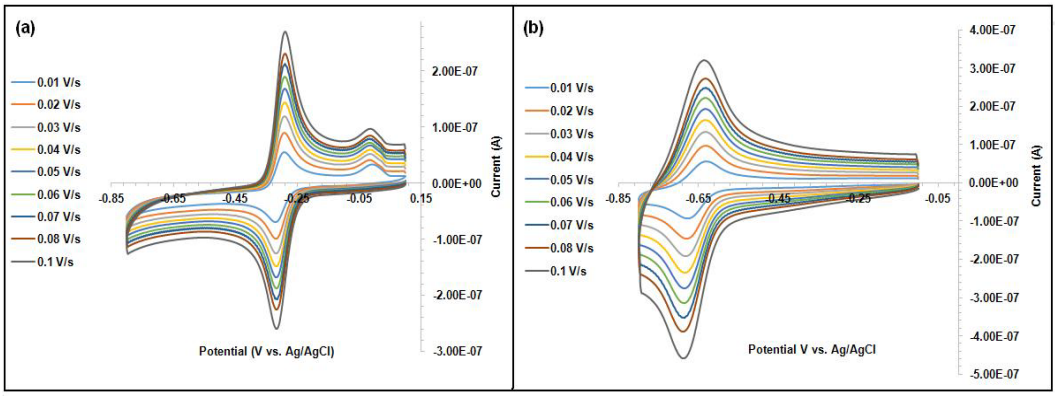

Figure 3-11 Effect of the scan rate on the cyclic voltammograms for the reduction of 0.1 mM Fl^{2+} in water at a glassy carbon disc electrode (2.0 mm dia.). Supporting electrolyte was 0.1 M Na_2SO_4 adjusted at a pH 3.0 (a) and 9.0 (b) respectively. Scan rates were varied from 0.01 to 0.1 V/s.

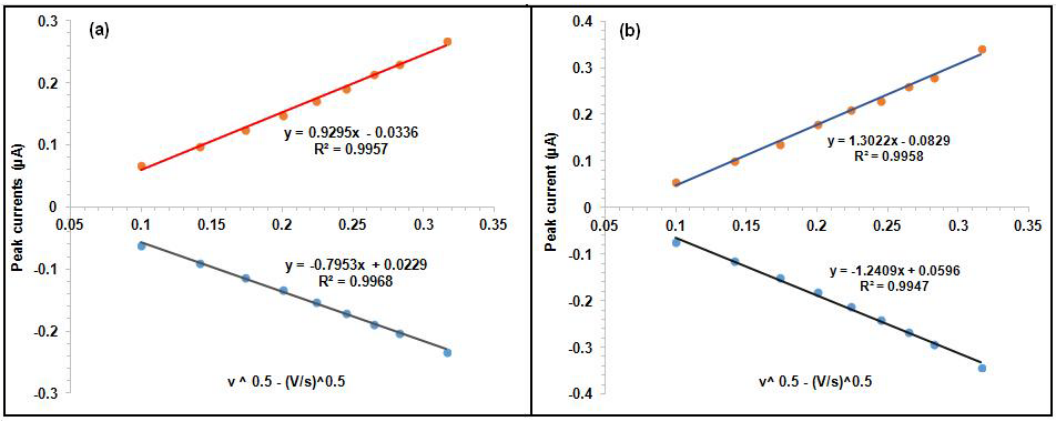

Figure 3-12 Dependence of the cathodic and anodic peak current versus the square root of scan rate for pH 3.0 (a) and pH 9.0 (b).

Notice that in Figure 3-11, the shape of the main voltammetric redox process at both pHs resembles a purely diffusion-controlled electrochemical process. To ascertain that the Fl^{2+} reduction follows a mass transport- controlled or a surface-controlled process, the dependency of the cathodic and anodic peak currents of CVs (from Figure 3-11) are shown in Figure 3-12 for both pHs as a function of the square root of scan rate.

The graphs show that both the anodic and cathodic peak current vary linearly with respect to the square root of scan rate, which indicates that Fl^{2+} reduction is a mass – transport – controlled process.[3]

3-4-2 Effect of pH on the Voltammetric Behavior of Fl^{2+}

Figure 3-13 compares cyclic voltammograms recorded on a GCE at different pH values and it explains that the compound exhibits a single redox couple in the pH range from 1 to 10. The different pHs were obtained by addition of sodium hydroxide (NaOH) and sulfuric acid (H_2SO_4), and then solutions were purged with N_2 to prevent the interference of the O_2 just before recording the respective CV for each sample. Again and in similarity with the data obtained on a gold electrode, the increase in the pH makes that the compound's reduction and oxidation peaks are shifted towards negative potentials, indicating that the compound redox reaction is definitively proton concentration dependent.

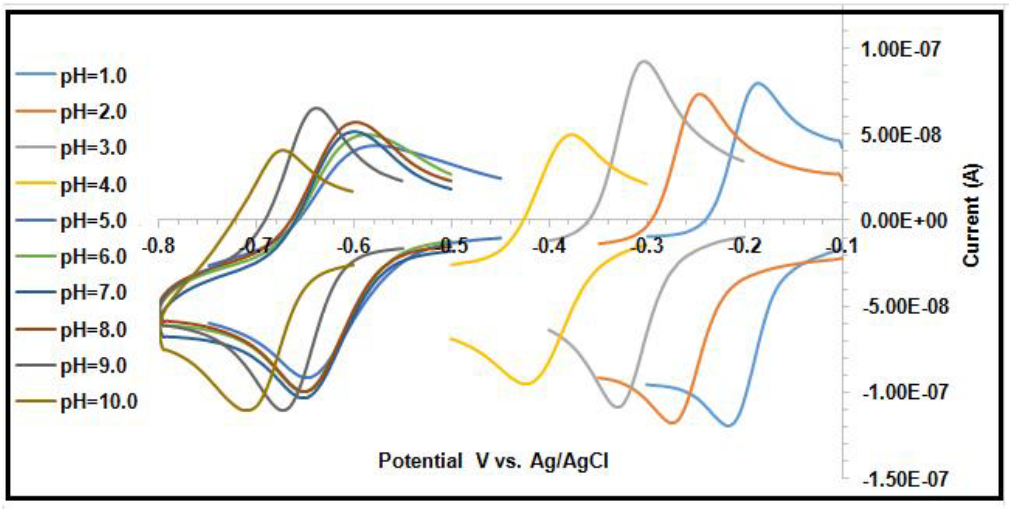

Figure 3-13 Effect of pH on the cyclic voltammograms of Fl^{2+} (0.1 M) at a glassy carbon electrode in an aqueous solution adjusted to selected pHs in the range 1 to 10. In all cases the scan rate was kept at 0.02 V/s.

To determine the number of electrons and protons transferred in the process, the dependency of formal potential [$E^{\circ\prime} = (E_{pc} + E_{pa}) / 2$][3] of redox reaction on the pH of supporting electrolyte for the compound is presented in Figure 3-14. Three regions were obtained after processing the data from Figure 3-13. At acidic pH (< 4) the slope of the formal potential vs. pH is 66 mV per pH unit which indicates two electrons -two protons process (see the corresponding equations inserted in Figure 3.12). At pH more basic than pH 7, the slope of formal potential vs. pH is 33 mV per pH unit which corresponds to an electrode process including two electrons and one proton. This data is in good agreement with that obtained on a gold electrode (shown in Fig. 3-7).

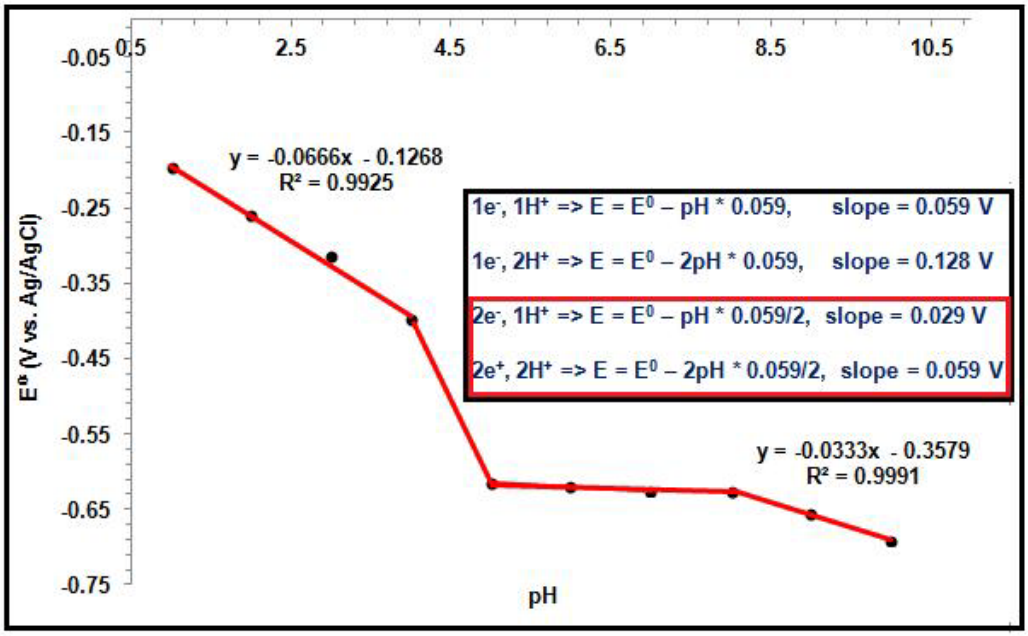

Figure 3-14 Dependence of FI^{2+} formal potential with respect the pH of the supporting electrolyte and in the pH range from 1 to 10. From the slope in different pH ranges, the number of electrons and protons involved in the respective reaction can be obtained as indicated by the equations in the insert box.

3-4-3 Spectroelectrochemical Study of the Fl^{2+}

Spectroelectrochemistry provides a method for correlating the electrochemical processes with the absorption data and thus directly observing the spectral evolution associated with speciation occurring during electroreduction/electrooxidation processes.[3] Thus, to enable spectroscopic determination of the species formed during the electroreduction of Fl^{2+}, a series of UV-Vis spectroelectrochemical experiments was carried out. Figure 3-15 shows UV-Vis spectroelectrochemical measurements of 2.5 mM Fl^{2+} compound in an aqueous solution of 0.1 M sodium sulfate at pH 7.0. These measurements were obtained in the transmittance mode and show all the species that are generated during a slow potential scan (5mV/s) in the thin-layer region next to a gold minigrid working electrode. The top frame of Figure 3-15 corresponds to the negative-going scan (reduction) and the bottom frame contains the spectra recorded during the subsequent, positive-going scan (oxidation). Arrows in each frame indicate the evolution of the corresponding spectral peaks as a function of potential. A comparison of the spectra in the negative- and positive-going scans shows that the electrochemical process is completely reversible.

The information from spectra in Figure 3-15 was processed further to obtain the difference absorption spectra (ΔA) which is presented in Figure 3-16. This ΔA is in fact defined as $A_E - A_{Ei}$ (with A_E corresponding to the spectrum at a certain potential E) and thus by subtracting the Fl^{2+} spectrum (recorded at the initial potential E_i of the voltammetric scan), the spectral changes incited by the potential can be more clearly observed (as they are presented in Figure 3-16).

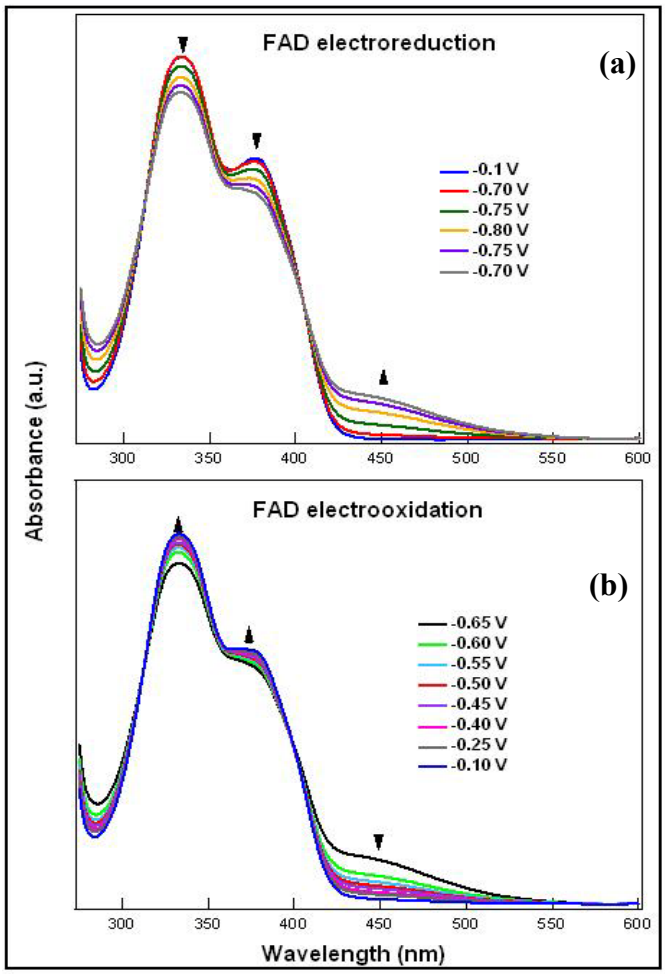

Figure 3-15 Spectroelectrochemistry of Fl^{2+} (2.5 mM) at pH 7 using a thin-layer cell with a gold mesh as working electrode. Spectra were collected during a cyclic potential scan at 5 mV/s in the -0.1 V to -0.8 V potential range. The evolution of the Fl^{2+} electronic spectra during the electroreduction (a) and the subsequent electrooxidation (b) indicates an electrochemical reversible process which is able to reach the initial Fl^{2+} spectrum at the end of the potential cycle.

The series of spectra at pH 9 is quite similar to those obtained at pH 7 which are not shown here. In spectra of Figure 3-16, bands pointing up correspond to species

formed and those pointing down are of the initial specie which is progressively disappearing as the electroreduction takes place. Considering each frame in detail, we can see on the top part of Figure 3-16 that the first spectrum corresponds to the Fl^{2+} compound as starting material, with two main bands located at 335 and 380 nm respectively. These bands are of similar intensity at pH 9 (spectra a) and 7 (not shown) but that is not the case for pH 3 (spectra b). The intensity of the 335 nm band is significantly higher at pH 3 than at other pHs which indicates the conversion (disappearance) of HFl^- to H_2Fl. Concomitantly, at pH 3 the increase of the band at 276 nm corroborates the formation of H_2Fl in agreement with other references. The band at 435 nm is assigned to formation of HFl which was detected at all pHs. This band grows with two companion bands at 274 and 291 nm. The intensity of 435 nm band is higher at pH 3 which is indicating a favorable formation of HFl as it would be the case of a comproportionation reaction eq. (3.2).

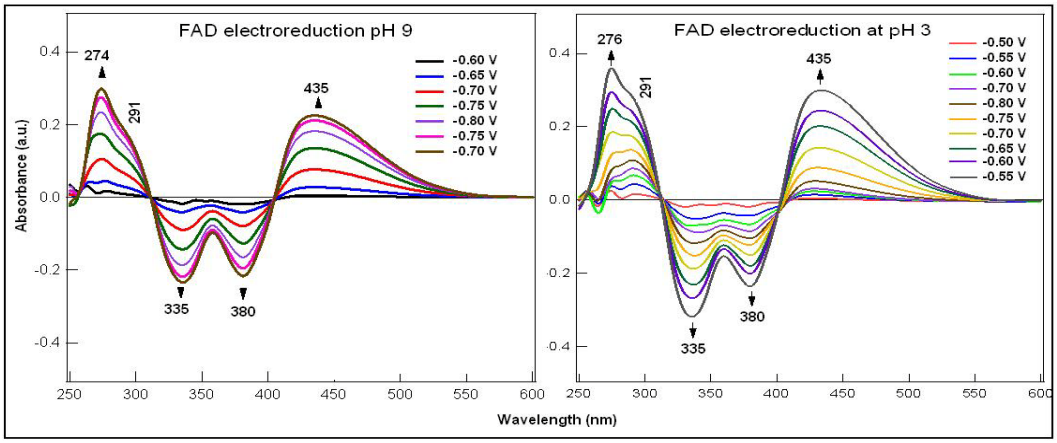

Figure 3-16 Difference absorption spectra, ΔA, obtained in situ during the electroreduction of Fl^{2+} at pH 9 (left) and 3 (right) are shown in the spectral range from 250 to 600 nm. The spectrum at pH 9 is quite similar to that obtained at pH 7 which is not shown for the sake of conciseness.

In aqueous or protic organic solvents, Fl is reported to be reduced in a two-electron reduction process.[73] However, due to the 1,3-disubstitution of Fl^{2+}, our compound could not act as a proton donor in comparison with published Fl references. Fl^{2+} redox potential vs. pH graph indicates $2e^-$, $1H^+$ at higher pH (> 7) and $2e^-$, $2H^+$ at low pHs (< 4). Therefore we postulate the following pH dependent mechanism (shown in Figure 3-17) which includes comproportionation reactions (C_1 & C_2).

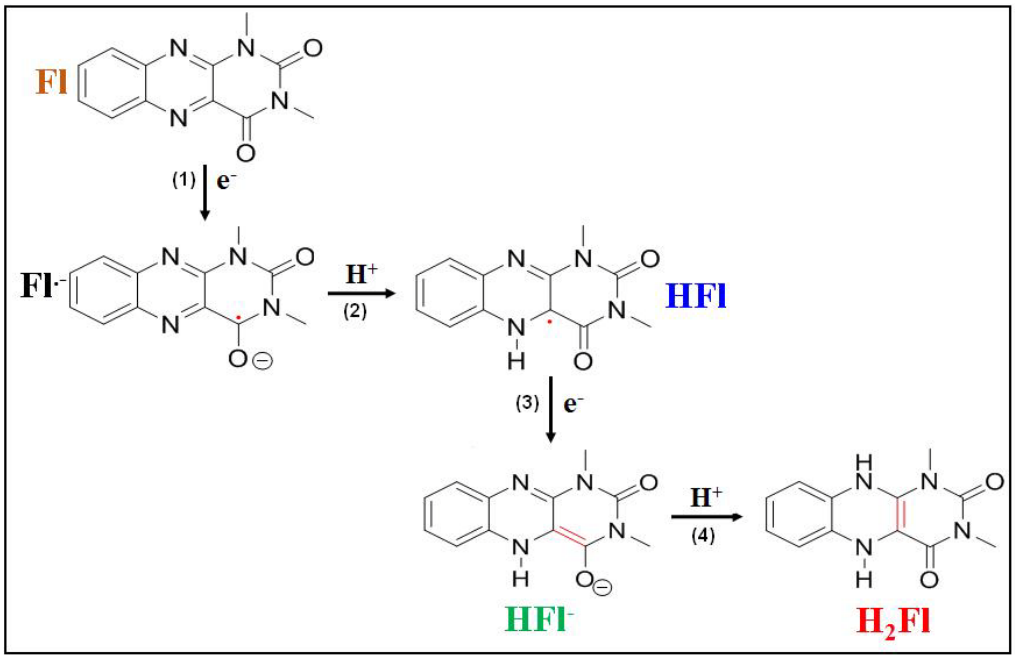

Figure 3-17 Box diagram of Fl^{2+} showing the formation of different species after two electrons and two protons process.

For the mechanism it is concluded that the initial electron transfer produces the radical anion, $Fl^{\cdot -}$ which underwent a rapid intermolecular proton transfer from the proton donor in the bulk solution, meaning the aqueous media, to form the neutral radical, HFl. After the proton coupled electron transfer, HFl was able to be further reduced to HFl^-. Once this step is reached, the pH of the solution plays an important role. In basic

solutions (>7) the reaction will not go further to get protonated to H_2Fl instead it will react with the starting species (Fl) in a comproportionation reaction (eq. (3.1)) to form the HFl species. In acidic media (<4), and because of the sufficient amount of protons in the system, HFl^- is protonated to reach H_2Fl. And then in another comproportionation reaction H_2Fl (eq. (3.2)) will react with the starting material (Fl) to form HFl. Therefore HFl is the dominant species which is formed in all pHs and is indicated by an spectral band peaking at 435 nm (see Figure 3-16).

At pH (>7), reactions 1-3 (as illustrated in Figure 3-17) and comproportionation reaction C_1 (eq. (3.1)) occurs,

$$HFl^- + Fl \overset{k^\circ_{C1}}{\leftrightarrow} HFl + Fl^- \quad (3.1)$$

At pH (<4), reactions 1-4 (as shown in Figure 3-17) and C_2 (eq. (3.2)) happens.

$$H_2Fl + Fl \overset{k^\circ_{C2}}{\leftrightarrow} 2HFl \quad (3.2)$$

Assignment for the species that were formed and for the species that were disappear is demonstrated in Table 3.1.

Table 3-1 Spectral bands associated to Fl^{2+} and its electroreduced and protonated species.

Species	Wavelength (nm)				
Fl			335	380	
HFl	274	291			435
HFl^-			335		
H_2Fl	276				

3-4-4 Electrocatalytic Activity of Fl^{2+} for Oxygen Reduction

Electrocatalytic activity for oxygen reduction reaction (ORR) is mainly accompanied with modified electrodes most of them containing Pt nanoparticles, either

by themselves or as binary composites containing Pt-Au or Pt-Pd nanoclusters in conjunction with carbon black. These nanocomposites containing noble metal entities are the most active catalysts for the conversion of oxygen to water.[128,129] However, with the aim to decrease the cost of using noble metal composites, several organic molecules have also been searched as electrocatalysts for ORR and some of them present significant electrocatalytic activity.[125,130]

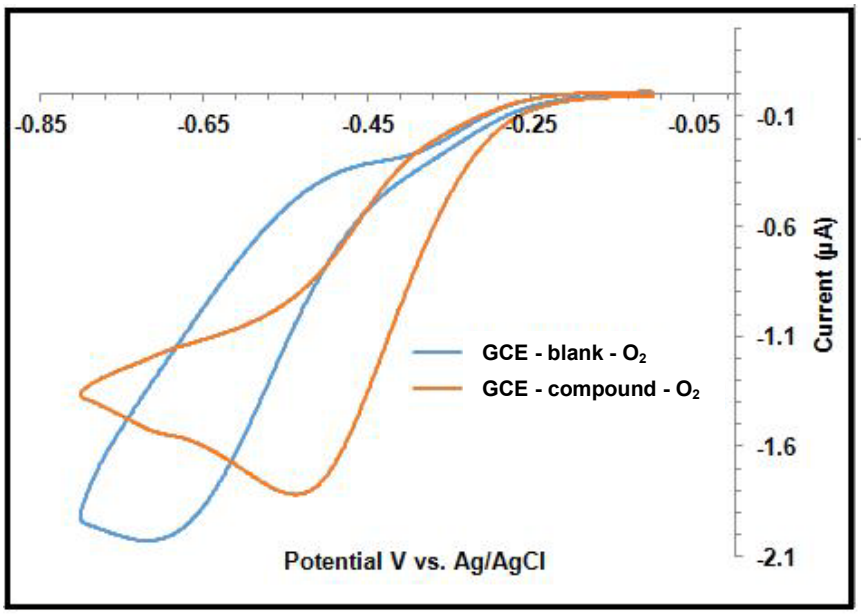

Figure 3-18 Cyclic voltammograms of a GCE in 0.1 M Na_2SO_4 saturated with O_2 containing (red trace) and without (blue trace) 0.1 mM Fl^{2+} to demonstrate the behavior of in the compound in the presence of O_2 for the scan rate of 0.02 V/s.

To investigate the electrocatalytic activity of Fl^{2+} in the oxygen electroreduction reaction, cyclic voltammetry on a GCE was performed in an O_2 saturated solution containing 0.1 M Na_2SO_4 in the presence (red trace) and absence (blue trace) of 0.1 mM Fl^{2+} (represented in Figure 3-18). In the presence of Fl^{2+} the oxygen reduction reaction occurs at more positive potentials suggesting Fl^{2+} has mediated the electrocatalytic

reduction of O_2. In fact, a positive potential shift of ca. 300 mV is promoted by the presence of the Fl^{2+} in the solution thus clearly confirming that this compound is a homogeneous electrocatalyst for the ORR.

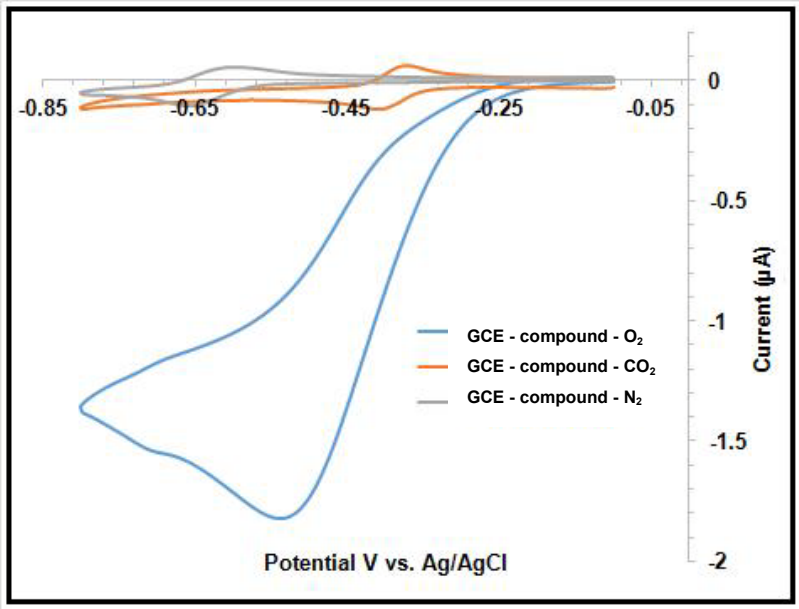

Figure 3-19 Cyclic voltammograms of a GCE in 0.1 M Na_2SO_4 containing 0.1mM Fl^{2+} saturated with O_2, (blue trace), CO_2 (red trace and N_2 (grey trace) suggesting the ability of the Fl^{2+} for the electrocatalytic reduction of O_2.

To compare the behavior of Fl^{2+} under the effect of saturation of the electrolyte with different gases (N_2, O_2 and CO_2), three voltammograms are compared in Figure 3-19. The difference between the redox potentials in the electrolyte which is saturated with N_2 and CO_2 directly corresponds to the pH effect; by dissolution of CO_2 in the electrolyte, its pH changes from about 7.0 to 5.5 and this change in the pH was resulted the shift in the redox potential. The large increase in the cathodic peak in the electrolyte that is saturated with O_2 and alternatively the decrease in the anodic peak in the voltammogram

shows the electrocatalytic activity for reduction of O_2. Contrarily, the Fl^{2+} compound was found not electrocatalytic active for the reduction of carbon dioxide.

3-4-5 Fl^{2+} Stability for Electrocatalytic Reduction of Oxygen

In order to obtain information about the stability of Fl^{2+}, CV experiment was performed in a 0.1 M Na_2SO_4 solution containing 0.1 mM Fl^{2+} saturated with oxygen. Two different experiments were carried out one for 8 and the other one for 15 cycles as it is displayed in Figure 3-20a and b. The results have demonstrated that the compound is stable after long cycles of scanning and no deformation on the peaks were observed.

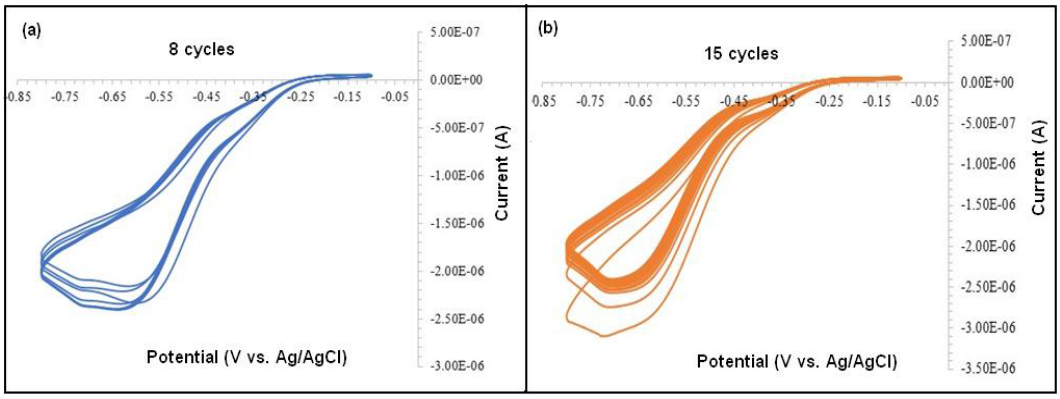

Figure 3-20 Cyclic voltammogram of glassy carbon electrode in 0.1 M Na_2SO_4 solution saturated with O_2, containing 0.1 mM Fl^{2+} after 8 (a) and 15 (b) cycles of scanning showing the stability of Fl^{2+} for O_2 reduction.

3-5 Conclusion

The electrochemical behavior of a newly synthesized compound, 1,3-diamine Flavin (Fl^{2+}), was investigated using three different electrode materials including, gold, copper/copper oxide and glassy carbon electrode. Glassy carbon electrode without any modification was chosen to be the best electrode material for this study. This compound showed a redox process located at -0.63 V vs. Ag/AgCl. This reduction process was

mass-transport-controlled as determined by the graph of the peak currents versus the square root of the potential scan rate. Electrochemical data associated with the effect of pH on the voltammetric peak potential of the compound pointed out to a proton dependent process involving two electrons and either one- or two protons depending on the availability of the protons (i.e. pH) in the system.

Spectroelectrochemistry illustrated an in depth study of the mechanism for these electron and proton transfer processes by identifying the respective reduced and protonated species. Finally the activity of the Fl^{2+} compound for the ORR and its high stability in the presence of O_2 in the system were investigated and the compound demonstrated an electrocatalytic activity for O_2 reduction. These results are all in agreement with the mechanisms and values which have been reported in recent years.[73,77,82,91,120,131,132]

References

1. Atkins, P.; Jones, L. *Chemical Principles: The Quest for Insight;* W. H. Freeman: 2004; Vol. 4, pp 1024.

2. Harris, D. C. *quantitative chemical analysis;* Freeman & Company, W. H.: 2010; Vol. 8, pp 750.

3. Bard, A.; Faulkner, L. *Electrochemical Methods: Fundamentals and Applications;* John Wiley & Sons, Inc: 2001; Vol. 2, pp 864.

4. Averill, B.; Eldredge, P. *Chemistry: principles, patterns and applications;* Prentice Hall: 2007; Vol. 1, pp 1250.

5. Zoski C. *Handbook of Electrochemistry;* Elsevier: 2006; Vol. 1, pp 934.

6. BACi bulk electrolysis cell. *http://www.basinc.com/products/ec/bulk.php* (accessed 09/25, 2013).

7. Rajeshwar, K.; McConnell, R.; Licht S. *Solar Hydrogen Generation: Toward a Renewable Energy Future;* Springer: 2008; pp 318.

8. Kissinger, P.; Heineman, W. R. *Laboratory Techniques in Electroanalytical Chemistry;* CRC press: 1996; Vol. 2, pp 1008.

9. Spectroelectrochemical cell. *http://www.basinc.com/products/ec/sec.php* (accessed 09/25, 2013).

10. Honda, K. *J. Photochem. Photobiol. A.* **2004***, 166*, 63-68.

11. Becqerel, A. E. **1839***, 9*, 561-567.

12. Nozik, A. J. *Annu. Rev. Phys. Chem.* **1978***, 29*, 189-222.

13. Rajeshwar, K. *J. Appl. Electrochem.* **1995***, 25*, 1067-1082.

14. Rajeshwar, K. *Spectroscopy* **1993***, 9*, 16.

15. Pelizzetti, E.; Serpone, N. *NATO ASI Series* **1986***, C174, 111*.

16. Schiavello, M. *NATO ASI Series* **1988***, C237*.

17. Pelizzetti E.; Schiavello, M. *NATO ASI Series* **1991**.

18. Ollis, D. F.; Al-Ekabi, H. *Proceedings of the First International Conference on TiO_2 Photocatalysic Purification and Treatment of Water and Air;* Elsevier: Amsterdam, 1993.

19. Helz, G. R.; Zepp, R. G.; Crosby, D. G. *Aquatic and surface photochemistry;* Lewis Publishers: Boca Raton, FL, 1994.

20. Ollis, D. F. *Environ. Sci. Technol.* **1985***, 19*, 480.

21. Pelizzetti, E.; Minero, C.; Maurino, V. *Adv. Colloid. Interfac. Sci.* **1990***, 32*, 271.

22. Ollis, D. F.; Pelizzetti, E.; Serpone, N. *Environ. Sci. Technol.* **1991***, 25*, 1523.

23. Fox, M. A. *Chem. Tech.* **1992**, 680.

24. Matthews, R. W. *Pure Appl. Chem.* **1992***, 64*, 1285.

25. Schiavello, M. *Electrochim. Acta* **1993***, 38*, 11.

26. Legrini, O.; Oliveros, E.; Braun, A. M. *Chem. Rev.* **1993***, 93*, 671.

27. Blake, D. M. *National Renewable Energy Laboratory Report,* **1994***, NREL/TP-430-6084*.

28. Gratzel, M. *Nature* **2001***, 414*, 338-344.

29. U.S. Environmental Protection Agency Climate change: Greenhouse emissions. *http://www.epa.gov* (accessed 02/15, 2012).

30. United States Environmental Protection Agency national green house gas emissions. *http://www.epa.gov/climatechange/ghgemissions/usinventoryreport.html* (accessed 09/03, 2013).

31. Jitaru, M. *J. Univ. Chem. Technol. Metal.* **2007***, 42*, 333-344.

32. Ghadimkhani, G.; de Tacconi, N. R.; Chanmanee, W.; Janaky, C.; Rajeshwar, K. *Chem. Commun.* **2013***, 49*, 1297-1299.

33. Gattrell, M.; Gupta, N.; Co, A. *J Electroanal. Chem.* **2006***, 594*, 1-19.

34. Hori, Y.; Kikuchi, K.; Suzuki, S. *Chem. Lett.* **1985**, 1695-1698.

35. Hori, Y.; Kikuchi, K.; Murata, A.; Suzuki, S. *Chem. Lett.* **1986**, 897-898.

36. Duba, P.; Brisard, G. M. *J Electroanal. Chem.* **2005***, 582*, 230-240.

37. Yano, H.; Tanaka, T.; Nakayama, M.; Ogura, K. *J. Electroanal. Chem.* **2004***, 565*, 287-293.

38. Aydin, R.; Koleli, F. *J. Electroanal. Chem.* **2002***, 535*, 107-112.

39. Schrebler, R.; Cury, P.; Suarez, C.; Muoz, E.; Gomez, H.; Cordova, R. *J. Electroanal. Chem.* **2002***, 533*, 167-175.

40. Schrebler, R.; Cury, P.; Herrera, F.; Gomez, H.; Cordova, R. *J. Electroanal. Chem.* **2001***, 516*, 23-30.

41. Brisard, G. M.; Camargo, A. P. M.; Nart, F. C.; Iwasita, T. *Electrochem. Commun.* **2001***, 3*, 603-607.

42. Tsubone, K.; Tanaka, A.; Fudeko, K.; Masahiro, A.; Yoshio, A.; Makoto, A. Bulletin of the Faculty of Human Environmental Science. **2005***, 36*, 13-21.

43. Lee, J.; Tak, Y. *Electrochim. Acta* **2001***, 46*, 3015-3022.

44. Li, H.; Oloman, C. *J. Appl. Electrochem.* **2006***, 36*, 1105-1115.

45. Li, H.; Oloman, C. *J. Appl. Electrochem.* **2007***, 37*, 1107-1117.

46. Jitaru, M.; Lowy, D. A.; Toma, M.; Toma, B. C.; Oniciu, L. *J. Appl. Electrochem.* **1997***, 27*, 875-889.

47. Koleli, F.; Ropke, T.; Hamann, C. H. *Electrochim. Acta* **2003***, 48*, 1595-1601.

48. Ohmori, T.; Nakayama, A.; Mametsuka, H.; Suzuki, E. *J. Electroanal. Chem.* **2001***, 514*, 51-55.

49. Kaneco, S.; Iiba, K.; Hiei, N.; Ohta, K.; Mizuno, T.; Suzuki, T. *Electrochim. Acta* **1999***, 44*, 4701-4706.

50. Kaneco, S.; Iwao, R.; Iiba, K.; Ohta, K.; Mizuno, T. *Energy* **1998***, 23*, 1107-1112.

51. Hirota, K.; Tryk, D. A.; Hashimoto, K.; Okawa, M.; Fujishima, A. In *Photoelectrochemical reduction of highly concentrated CO2 in methanol solution;* T. Inui, M. Anpo, K. Izui,S.Yanagida and T.Yamaguchi, Ed.; Studies in Surface Science and Catalysis; Elsevier: 1998; Vol. olume 114, pp 589-592.

52. Kaneco, S.; Iiba, K.; Ohta, K.; Mizuno, T.; Saji, A. *Electrochim. Acta* **1998***, 44*, 573-578.

53. Welford, P. J.; Brookes, B. A.; Wadhawan, J. D.; McPeak, H. B.; Hahn, C. E. W.; Compton, R. G. *J. Phys. Chem. B* **2001***, 105*, 5253-5261.

54. Isaacs, M.; Canales, J. C.; Riquelme, A.; Lucero, M.; Aguirre, M. J.; Costamagna, J. *J. Coordination Chem.* **2003***, 56*, 1193-1201.

55. Begum, A.; Pickup, P. G. *Electrochem. Commun.* **2007***, 9*, 2525-2528.

56. A. Rios-Escudero, M. Isaacs, M. Villagrán, J. Zagal and J. Costamagna *The Journal of the Argentine Chemical Society* **2004***, 92*, 63.

57. Magdesieva, T. V.; Zhukov, I. V.; Kravchuk, D. N.; Semenikhin, O. A.; Tomilova, L. G.; Butin, K. P. *Russian Chemical Bulletin* **2002***, 51*, 805-812.

58. Ikeda, S.; Shiozaki, S.; Susuki, J.; Ito, K.; Noda, H. Electroreduction of CO2 using Cu/Zn oxides loaded gas diffusion electrodes. *Advances in Chemical Conversions for Mitigating Carbon Dioxide Proceedings of the Fourth International Conference on Carbon Dioxide Utilization* **1998***, 114*, 225-230.

59. Nakaoka, K.; Ueyama, J.; Ogura, K. *J. Electrochem. Soc.* **2004***, 151*, C661-C665.

60. Solar cells for full spectrum efficiency. *http://www.freerepublic.com/focus/news/803234/posts* (accessed 02/25, 2012).

61. Barton Cole, E.; Bocarsly, A. B. In *Photochemical, Electrochemical, and Photoelectrochemical Reduction of Carbon Dioxide;* Michele Aresta, Ed.; Carbon Dioxide as Chemical Feedstock; Wiley-VCH Verlag GmbH & Co. KGaA: 2010; pp 291-316.

62. Kumar, B. F.; Llorente, M. F.; Froehlich, J. F.; Dang, T. F.; Sathrum A FAU - Kubiak, Clifford,P.; Kubiak, C. P. *Annu. Rev. Phys. Chem.* **2012**, *63,* 541-569.

63. Boston, D. J.; Huang, K. L.; De Tacconi, N. R.; Myung, N.; MacDonnell, F. M., Rajeshwar, K. In *Electro- and Photocatalytic Reduction of CO_2: The Homogeneous and Heterogeneous Worlds Collide?* Photoelectrochemical Water Spliting: Challenges and New Perspectives; 2013.

64. Somasundaram, S.; Raman Nair Chenthamarakshan, C.; de Tacconi, N. R.; Rajeshwar, K. *Int. J. Hydrogen Energy* **2007***, 32*, 4661-4669.

65. Eggins, B. R.; Robertson, P. K. J.; Murphy, E. P.; Woods, E.; Irvine, J. T. S. *J. Photochem. Photobiol. A.* **1998***, 118*, 31-40.

66. Wang, X.; Hanson, J. C.; Frenkel, A. I.; Kim, J.; Rodriguez, J. A. *J. Phys Chem. B* **2004***, 108*, 13667-13673.

67. Methanol manufacturing. *http://www.ttmethanol.com/web/methprocess.html* (accessed 02/15, 2012).

68. Institute for the Analysis of Global Security Methsnol sources. *http://www.iags.org/methanolsources.htm* (accessed 02/20, 2012).

69. Paracchino, A.; Laporte, V.; Sivula, K.; Gratzel, M.; Thimsen, E. *Nat. Mater.* **2011***, 10*, 456-461.

70. Paracchino, A.; Brauer, J. C.; Moser, J.; Thimsen, E.; Graetzel, M. *J. Phys. Chem. C* **2012***, 116*, 7341-7350.

71. Edwards, A. M. In *Chapter 1 General Properties of Flavins;* The Royal Society of Chemistry: 2006; Vol. 6, pp 1-11.

72. Blyth, A. W. *J. Chem. Soc. Trans.* **1879***, 35*, 530-539.

73. Tan, S. L. J.; Webster, R. D. *J. Am. Chem. Soc.* **2012***, 134*, 5954-5964.

74. Huynh, M. H., V.; Meyer, T. *J. Chem. Rev.* **2007***, 107*, 5004–5064.

75. Durliat, H.; Barrau, M. B.; Comtat, M. *Bioelectrochem. Bioenerget.* **1988***, 19*, 413-423.

76. Zayats, M. F.; Katz, E. F.; Willner, I. *J. Am. Chem. Soc.* **2002***, 124,* 2120-2121.

77. Kumar, S. A.; Chen, S. *Sensors Actuators B: Chem.* **2007***, 123*, 964-977.

78. Chen, S.; Liu, M. *Electrochim. Acta* **2006***, 51*, 4744-4753.

79. Lin, L. K.; Chen, S. M. *Biosensors Bioelectronics* **2006***, 21,* 1737-1745.

80. Shinohara, H.; Gratzel, M.; Vlachopoulos, N.; Aizawa, M. *J. Electroanal. Chem. Interfac. Electrochem.* **1991***, 321*, 307-320.

81. Erkang, W.; Jingdong, Z.; Qijin, C.; Shaojun, D. *J. Electroanal. Chem.* **1994***, 364*, 261-263.

82. Reeves, J. H.; Weiss, K. *J. Electroanal. Chem. Interfac. Electrochem.* **1987***, 217*, 65-78.

83. Birss, V. I.; Guha-Thakurta, S.; McGarvey, C. E.; Quach, S.; Vanasek, P. *J. Electroanal. Chem.* **1997***, 423*, 13-21.

84. Kamal, M. M.; Elzanowska, H.; Gaur, M.; Kim, D.; Birss, V. I. *J. Electroanal. Chem. Interfac. Electrochem.* **1991***, 318*, 349-367.

85. McGarvey, C.; Beck, S.; Quach, S.; Birss, V. I.; Elzanowska, H. *J. Electroanal. Chem.* **1998***, 456*, 71-82.

86. Kubota, L. T.; Gorton, L.; Roddick-Lanzilotta, A.; McQuillan, A. J. *Bioelectrochem. Bioenerget.* **1998***, 47*, 39-46.

87. Wang, Y.; Zhu, G.; Wang, E. *Anal. Chim. Acta* **1997***, 338*, 97-101.

88. Gorton, L.; Johansson, G. *J. Electroanal. Chem. Interfac. Electrochem.* **1980***, 113*, 151-158.

89. Miyawaki, O.; Wingard, L. B. *Biotechnol. Bioeng.* **1984***, 26*, 1364-1371.

90. Miyawaki, O.; Wingard Jr., L. *Biochimica et Biophysica Acta (BBA) - General Subjects* **1985***, 838*, 60-68.

91. Niemz, A.; Imbriglio, J.; Rotello, V. M. *J. Am. Chem. Soc.* **1997***, 119*, 887-892.

92. Rajeshwar, K.; de Tacconi, N. R.; Ghadimkhani, G.; Chanmanee, W.; Janaky, C. *Chem. Phys. Chem.* **2013***, 14*, 2251-2259.

93. Tacconi, N. R.; Rajeshwar, K.; Lezna, R. O. *J. Phys. Chem.* **1996***, 100*, 18234-18239.

94. Le, M.; Ren, M.; Zhang, Z.; Sprunger, P. T.; Kurtz, R. L.; Flake, J. C. *J. Electrochem. Soc.* **2011***, 158*, E45-E49.

95. Paracchino, A.; Brauer, J. C.; Moser, J.; Thimsen, E.; Graetzel, M. *J. Phys. Chem. C* **2012**.

96. Zhou, Y.; Switzer, J. A. *Scr. Mater.* **1998***, 38*, 1731-1738.

97. Golden, T. D.; Shumsky, M. G.; Zhou, Y.; VanderWerf, R. A.; Van Leeuwen, R. A.; Switzer, J. A. *Chem. Mater.* **1996***, 8*, 2499-2504.

98. Wang, L. C.; Tacconi, N. R.; Chenthamarakshan, C. R.; Rajeshwar, K.; Tao, M. *Thin Solid Films* **2007***, 515*, 3090-3095.

99. Somasundaram, S.; Raman, N. C.; de Tacconi, N. R.; Rajeshwar, K. *Int J Hydrogen Energy* **2007***, 32*, 4661-4669.

100. Jiang, X.; Herricks, T.; Xia, Y. *Nano. Lett.* **2002***, 2*, 1333-1338.

101. Park, Y.; Seong, N.; Jung, H.; Chanda, A.; Yoon, S. *J. Electrochem. Soc.* **2010***, 157*, K119-K124.

102. Dar, M.; Nam, S.; Kim, Y.; Kim, W. *J. Solid State Electrochem.* **2010***, 14*, 1719-1726.

103. Mohemmed Shanid, N. A.; Abdul Khadar, M.; Sathe, V. G. *J. Raman Spectrosc.* **2011***, 42*, 1769-1773.

104. Mao, Y.; He, J.; Sun, X.; Li, W.; Lu, X.; Gan, J.; Liu, Z.; Gong, L.; Chen, J.; Liu, P.; Tong, Y. *Electrochim. Acta* **2012***, 62*, 1-7.

105. Anonymous *http://www.chem.arizona.edu/massspec/intro_html/intro.html* (accessed 10/16, 2013).

106. Myung, N.; Wei, C.; de Tacconi, N. R.; Rajeshwar, K. *J. Electroanal. Chem.* **1993***, 359*, 307-313.

107. Bohannan, E. W.; Huang, L.; Miller, F. S.; Shumsky, M. G.; Switzer, J. A. *Langmuir* **1999***, 15*, 813-818.

108. Haller, S.; Jung, J.; Rousset, J.; Lincot, D. *Electrochim. Acta* **2012***, 82*, 402-407.

109. Wu, L.; Tsui, L.; Swami, N.; Zangari, G. *J. Phys. Chem. C* **2010***, 114*, 11551-11556.

110. Huang, L.; Peng, F.; Yu, H.; Wang, H. *Solid State Sciences* **2009***, 11*, 129-138.

111. Zheng, Z.; Huang, B.; Wang, Z.; Guo, M.; Qin, X.; Zhang, X.; Wang, P.; Dai, Y. *J. Phys. Chem. C* **2009***, 113*, 14448-14453.

112. Bessekhouad, Y.; Robert, D.; Weber, J. Photocatalytic activity of Cu_2O/TiO_2, Bi_2O_3/TiO_2 and $ZnMn_2O_4/TiO_2$ heterojunctions. *Catalysis Today; Environmental Applications of Photocatalysis, 3rd European Meeting on Solar Chemistry and Photocatalysis: Environmental Applications Environmental Applications of Photocatalysis* **2005***, 101*, 315-321.

113. Bockris, J. O.; Wass, J. C. *J. Electrochem. Soc.* **1989***, 136*, 2521-2528.

114. Rosen, B. A.; Salehi-Khojin, A.; Thorson, M. R.; Zhu, W.; Whipple, D. T.; Kenis, P. J. A.; Masel, R. I. *Science* **2011***, 334*, 643-644.

115. Zayats, M.; Katz, E.; Willner, I. *J. Am. Chem. Soc.* **2002***, 124*, 2120-2121.

116. Stine, K. J.; Andrauskas, D. M.; Khan, A. R.; Forgo, P.; Dasouza, V.,T.; Liu, J.; Friedman, R. M. *J. Electroanal. Chem.* **1999***, 472*, 147-156.

117. Noll, G.; Kozma, E.; Grandori, R.; Carey, J.; Schodl, T.; Hauska, G.; Daub, J. *Langmuir* **2006***, 22*, 2378-2383.

118. Noll, G. *J. Photochem. Photobiol. A.* **2008***, 200*, 34-38.

119. Wei, H.; Tan, H.; Zeng, Y. *Phys. Chem. Liq.* **2010***, 48*, 708-722.

120. Wei, H.; Omanovic, S. *Chem. Biodiv.* **2008***, 5*, 1622-1639.

121. Birss, V. I.; Hinman, A. S.; McGarvey, C. E.; Segal, J. *Electrochim. Acta* **1994***, 39*, 2449-2454.

122. Amadelli, R.; Molinari, A.; Vitali, I.; Samiolo, L.; Mura, G. M.; Maldotti, A. Photo-electro-chemical properties of TiO_2 mediated by the enzyme glucose oxidase. *Catalysis Today; Environmental Applications of Photocatalysis, 3rd European Meeting on Solar Chemistry and Photocatalysis: Environmental Applications Environmental Applications of Photocatalysis* 2005*, 101*, 397-405.

123. Shinohara, H.; Gratzel, M.; Vlachopoulos, N.; Aizawa, M. *J. Electroanal. Chem. Interfac. Electrochem.* **1991***, 321*, 307-320.

124. Garjonyte, R.; Malinauskas, A.; Gorton, L. *Bioelectrochem.* **2003***, 61*, 39-49.

125. Lo, P.; Kumar, S. A.; Chen, S. *Colloids and Surfaces B: Biointerfaces* **2008***, 66*, 266-273.

126. Chen, S.; Foss, F. W. *Org. Lett.* **2012***, 14*, 5150-5153.

127. Chen, S.; Hossain, M. S.; Foss, F. W. *Org. Lett.* **2012***, 14*, 2806-2809.

128. Tacconi, N. R.; Chenthamarakshan, C. R.; Rajeshwar, K.; Lin, W.; Carlson, T. F.; Nikiel, L.; Wampler, W. A.; Sambandam, S.; Ramani, V. *J. Electrochem. Soc.* **2008***, 155*, 1102-1109.

129. Tacconi, N. R.; Rajeshwar, K.; Chanmanee, W.; Valluri, V.; Wampler, W. A.; Lin, W.; Nikiel, L. *J. Electrochem. Soc.* **2010***, 157*, 147-153.

130. Chi, Q.; Dong, S. *J. Electroanal. Chem.* **1994***, 369*, 169-174.

131. Lin, K.; Chen, S. *Biosensors and Bioelectronics* **2006***, 21*, 1737-1745.

132. Male, R.; Samotowka, M. A.; Allendoerfer, R. D. *Electroanalysis* **1989***, 1*, 333-339.

Biographical Information

Ghazaleh Ghadimkhani received her PhD in Chemistry and Biochemistry (with specialization in Electrochemistry) from The University of Texas at Arlington in December 2013. She obtained her Bachelor of Science degree in Chemical Engineering from University of Tehran, Iran in August 2009.